VISIOPLASTICITY ANALYSIS OF ROD DRAWING

By
RAKESH SHARMA

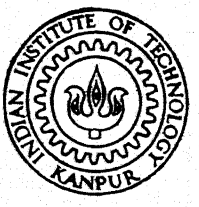

DEPARTMENT OF MECHANICAL ENGINEERING
N INSTITUTE OF TECHNOLOGY, KANPUR

AUGUST, 1980

VISIOPLASTICITY ANALYSIS OF ROD DRAWING

A Thesis Submitted
in Partial Fulfilment of the Requirements
for the Degree of
MASTER OF TECHNOLOGY

By
RAKESH SHARMA

to the
DEPARTMENT OF MECHANICAL ENGINEERING
INDIAN INSTITUTE OF TECHNOLOGY, KANPUR
AUGUST, 1980

C E R T I F I C A T E

This is to certify that the work entitled "VISIOPLASTICITY ANALYSIS OF ROD DRAWING" by Rakesh Sharma has been carried out under my supervision and has not been submitted elsewhere for a degree.

Dr. G.K. Lal
Professor
Department of Mechanical Engineering
I.I.T. Kanpur

ME-1986-M-SHA-VIS

ACKNOWLEDGEMENTS

I am extremely indebted to Dr. G.K. Lal for suggesting the present problem and devoting his invaluable time in guiding me throughout the course of this work.

I am also grateful to Dr. A. Ghosh for his helpful suggestions.

I would like to express my sincere thanks to Anil Srivastava for his constant help all along the preparation and writing up of this thesis.

Thanks are also due to Shashi Srivastava and Navin Mathur for their help, and to Mr. G.L. Misra for his flaw-less typing.

Last but not least, I am indebted to my wife without whose constant "nagging" this work may not have reached its present status.

I.I.T. Kanpur RAKESH SHARMA

L I S T O F F I G U R E S

N O M E N C L A T U R E

a	Deformed grid line
a_o	Undeformed grid line
α	Angle made by the tangent to aa_o with the x-axis
$d\epsilon_{ij}$	Strain increment tensor
d	Parameter relating strain increment tensor and deviatoric stress
$\delta\epsilon_I$	Linear strain invariant
δV	Volume of the material, mm^3
$\frac{\delta V}{V}$	Dilatation
E	Young's modulus
ϵ_x	Strain in the x direction
ϵ_y	Strain in the y direction
ϵ_z	Strain in the z direction
$\dot{\epsilon}_x$	Strain rate in x direction, per second
$\dot{\epsilon}_y$	Strain rate in y direction, per second
$\dot{\bar{\epsilon}}$	Strain rate
ϵ_{r_o}	Tensile or Compressive strain at an arbitrary point on the surface of the disc due to drawing force
$\epsilon_{r_o\ max}$	Maximum value of ϵ_{r_o}
F_x	Force in x direction, Kg.
F_y	Force in y direction, Kg.
F_z	Force in z direction, Kg.
ϕ'	Flow function, mm^3 per second
$\dot{\gamma}_{xy}$	Shear strain rate, per second

m	Poisson's ratio
P	Drawing force, Kg.
p	Hydrostatic pressure, Kg. per mm^2
r	Any arbitrary radius for the dynamometer from the centre of the boss
r_o	Radius of the dynamometer boss
r_1	Radius of the dynamometer disc
S	Distance between two nodes
σ_x	Stress in x direction, Kg per mm^2
σ_y	Stress in y direction, Kg per mm^2
σ_z	Stress in z direction, Kg per mm^2
σ'_{ij}	Deviatoric stress tensor
$\bar{\sigma}$	Effective flow stress
t	Thickness of the disc of the disc dynamometer
t_o	Distance between any two flow lines, mm.
τ_{yz}	Shear stress in x direction, Kg. per mm^2
τ_{xz}	Shear stress in y direction, Kg. per mm^2
τ_{xy}	Shear stress in z direction, Kg. per mm^2
u	Velocity in x direction, mm per second.
V	Volume of the material, mm^3
V_o	Drawing velocity, mm per second.
v	Velocity in y direction mm per second.
w	Deflection of the dynamometer boss due to drawing force
w_{max}	Maximum deflection of the boss due to drawing force

A B S T R A C T

of the

Dissertation on

VISIOPLASTICITY ANALYSIS OF ROD DRAWING

Submitted in Partial Fulfilment of

the Requirements for the Degree

of

MASTER OF TECHNOLOGY IN MECHANICAL ENGINEERING

by

RAKESH SHARMA

Department of Mechanical Engineering

Indian Institute of Technology, Kanpur

August 1980

Rod or wire drawing has been practiced by man since time immemorial but research in this particular field has been scanty and sporadic. The present work was aimed to study mechanics of rod drawing by visioplasticity technique and to compare the results so obtained with those obtained experimentally.

The visioplasticity technique suggested requires the flow pattern of the deforming material and from it the velocity field is obtained. The strain rates and stress can then be calculated by considering the equilibrium and plasticity equations. Flow patterns have been obtained by carrying out

rod drawing experiments with lead rods split exactly on the dimetral plane. One of the diametral planes was inscribed with fine parallel lines.

An HMT lathe was modified to work as a draw bench to draw lead rods through a split die fabricated to give 10 per cent reduction. Experiments were carried out at various drawing speeds under dry conditions. To obtain instantaneous values of drawing and separating forces simultaneously, a disc dynamometer was specially designed and fabricated.

A numerical technique was evolved to theoretically evaluate the velocity and the stress fields within the deforming region. Theoretical separating force was evaluated from the stress field thus obtained. Theoretical results show reasonably good agreement with the experimental values.

T A B L E O F C O N T E N T S

C H A P T E R - 1

INTRODUCTION

1.1 INTRODUCTION

Viscoplasticity is an experimental method for determining stresses and strain rates in a deforming body. In this method the velocity vector field is established by experiment and the stresses are calculated therefrom. This can be accomplished in a number of ways : for example, by placing a grid pattern on the merideian plane of a cylinder or on a plane at right angles to the metal movement, as in plane-strain problems, and observe its rate of distortion. The plane on which the grid lines are placed is photographed after each incremental forming step and the particle movement, as represented by the new positions of the grid line intersections, is observed.

A few such incremental steps are usually sufficient to obtain an adequate flow pattern. If the flow is nonsteady, only one small forming step can be used; otherwise the flow pattern will be incorrect. It must be observed that grids deformed in a finite step cannot be used in the analysis if the deformation is nonuniform. Having established the instantaneous particle flow field, as shown in Fig. 1.1(a), subsequent analysis will lead to the determination of stress and strain-rate patterns.

Let the velocity of a particular grid-line intersection be given by V and its components in the x,y coordinate directions by u and v, as shown in Fig. 1.1(b). It is assumed that it is possible to measure the velocity V and the angle of inclination of the velocity vector with the x-axis. Consiquently, u and v can be obtained for any desired point. (u and v are thus velocities and not displacements). If the points at which the velocities are known are sufficiently close together, it will be possible to prepare the following graphs :

u versus x; v versus x;
u versus y; v versus y.

Evaluation of the slopes of these curves at each desired coordinate point permits, the determination of the strain rates from

$$\dot{\epsilon}_x = \frac{\partial u}{\partial x} , \qquad (1.1)$$

$$\dot{\epsilon}_y = \frac{\partial v}{\partial y} \qquad (1.2)$$

$$\dot{\gamma}_{xy} = \frac{\partial v}{\partial x} + \frac{\partial u}{\partial y} \qquad (1.3)$$

For plane strain problems and problems of axial symmetry measurement of u and v and the determination of strain rate components on a central plane are sufficient for the evaluation of forces.

1.2 WIRE OR ROD DRAWING

Wire or rod drawing is a process of pulling a cylindrical work piece through conical die which results in the reduction of its cross section and increase in its length. The drawing operation may be accomplished with or without a back pull. If a back pull is applied to the bar or wire at its entrance section, it aids materially in the possible reduction per pass. Wire drawing is normally a cold working process in which close tolerances and a good surface finish can be produced in the drawn wire.

In order to resist wear, dies are usually made of tungsten carbide, but diamond dies are also used, especially for diameters below 1.4 mm (0.055 in.). The die profile affects the drawing force, and in industrial practice usually has a bevel-mouthed shape. In order to simplify analysis of forces, energy consumed,split forces etc. the die shape is generally assumed to be conical.

The early work in wire drawing was concerned principally with the relationships of drawing forces and power for various drawing conditions. Later, in 1928, G. Sachs [1] analysed wire drawing by the slab method and obtained a solution for the drawing stresses. Sporadic work on forces and deformation in wire drawing was reported over the years. Cook and Wistreich [2] measured the die pressure in wire drawing by the use of photo elastic methods. However, visioplasticity technique to predict the forces occuring during the process

of wire drawing has not been so far utilised.

In the present work an attempt has been made to predict by visioplasticity technique forces occuring during the process of rod drawing and to compare them with the instantaneous forces actually measured during the process.

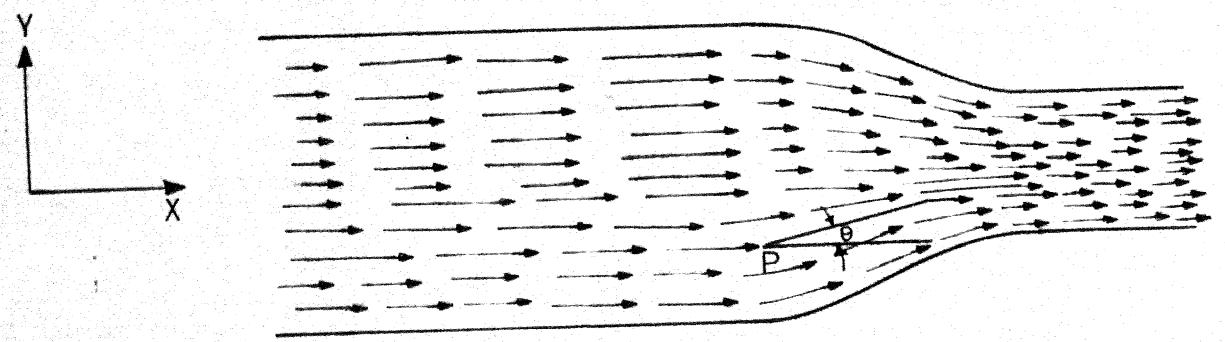

(a)

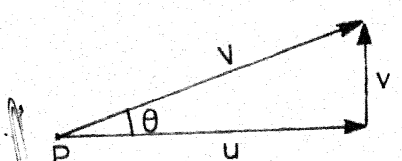

(b)

Fig. 1·1 Instantaneous velocity vectors in a plastic flow field
(a) Velocity vector field (b) Velocity vector components at P

C H A P T E R - 2

THEORY OF VISCOPLASTICITY

2.1 ANALYSIS

For static equilibrium summation of all the forces (F) in each of the three perpendicular direction is individually equal to zero. Expressed in symbolic form,

$$\Sigma F_x = \Sigma F_y = \Sigma F_z = 0 \qquad (2.1)$$

Investigation of the particular condition $\Sigma F_x = 0$ results in

$$(\sigma_x + \frac{\partial \sigma_x}{\partial x} dx)\, dy\, dz + (\tau_{zx} + \frac{\partial \tau_{zx}}{\partial z} dz)\, dx\, dy$$

$$+ (\tau_{yx} + \frac{\partial \tau_{yx}}{\partial y} dy)\, dx\, dz - \sigma_x\, dy\, dz$$

$$- \tau_{zx}\, dy\, dx - \tau_{yx}\, dx\, dz = 0 \qquad (2.2)$$

where σ and τ represent direct and shear stress values respectively. Simplification of equation (2.2) results in

$$\frac{\partial \sigma_x}{\partial x} + \frac{\partial \tau_{yx}}{\partial y} + \frac{\partial \tau_{zx}}{\partial z} = 0; \quad \Sigma F_x = 0 \qquad (2.3)$$

Similarly it can be shown that

$$\frac{\partial \tau_{xy}}{\partial x} + \frac{\partial \sigma_y}{\partial y} + \frac{\partial \tau_{zy}}{\partial z} = 0; \quad \Sigma F_y = 0 \qquad (2.4)$$

and

$$\frac{\partial \tau_{xz}}{\partial x} + \frac{\partial \tau_{yz}}{\partial y} + \frac{\partial \sigma_z}{\partial z} = 0; \quad \Sigma F_z = 0 \qquad (2.5)$$

For the case of plane strain, the equilibrium equations (2.3), (2.4) and (2.5) reduce to

$$\frac{\partial \sigma_x}{\partial x} + \frac{\partial \tau_{xy}}{\partial y} = 0 \qquad (2.6)$$

$$\frac{\partial \sigma_y}{\partial y} + \frac{\partial \tau_{xy}}{\partial x} = 0 \qquad (2.7)$$

$$\frac{\partial \sigma_z}{\partial z} = 0 \qquad (2.8)$$

After plastic deformation of a rigid plastic material, its volume remains constant, which means that the sum of strains (ϵ) in the three perpendicular directions is zero. (The linear strain invariant $\delta\epsilon_I$ takes the following values.

i) If the strains are plastic, then $\delta\epsilon_I = \delta\epsilon_m$ and the mean strain becomes

$$3\delta\epsilon_I = \delta\epsilon_x + \delta\epsilon_y + \delta\epsilon_z = \epsilon_x + \epsilon_y + \epsilon_z = \frac{\delta V}{V} \qquad (2.9)$$

where V is the unit volume of the material and $\delta V/V$ is known as the dilatation. However, if the strains are plastic we may write

$$\delta\epsilon_x + \delta\epsilon_y + \delta\epsilon_z = 0 \qquad (2.10)$$

or

$$\delta\epsilon_1 + \delta\epsilon_2 + \delta\epsilon_3 = 0 \qquad (2.11)$$

Analogous equations also hold for strain rates and finite strains; that is

$$\dot{\epsilon}_x + \dot{\epsilon}_y + \dot{\epsilon}_z = 0 \qquad (2.12)$$

or

$$\epsilon_x + \epsilon_y + \epsilon_z = 0 \tag{2.13}$$

In case of plane strain, $\dot{\epsilon}_z = 0$

$$\dot{\epsilon}_x + \dot{\epsilon}_y = 0 \tag{2.14}$$

or

$$\dot{\epsilon}_x = - \dot{\epsilon}_y \tag{2.15}$$

Strain increment tensor $d\epsilon_{ij}$ is related to deviatoric stress tensor σ'_{ij} by the equation

$$d\epsilon_{ij} = d\lambda \ \sigma'_{ij} \tag{2.16}$$

where $d\lambda$ is a parameter which usually changes during the deformation, or

$$\dot{\epsilon}_{ij} = \dot{\lambda} \ \sigma'_{ij} \tag{2.17}$$

where

$$\dot{\lambda} = \frac{3}{2} \ \frac{\bar{\dot{\epsilon}}}{\bar{\sigma}} \tag{2.18}$$

Here the effective strain rate ($\bar{\dot{\epsilon}}$) and the effective flow stress ($\bar{\sigma}$) are defined as

$$\bar{\dot{\epsilon}} = \frac{2}{3} \sqrt{\frac{1}{2} \ (\dot{\epsilon}_x - \dot{\epsilon}_y)^2 + (\dot{\epsilon}_y - \dot{\epsilon}_z)^2 + (\dot{\epsilon}_z - \dot{\epsilon}_x)^2 \ + \frac{3}{4} \ \dot{\gamma}^2_{xy}} \tag{2.19}$$

and

$$\bar{\sigma} = \sqrt{\frac{1}{2} \ (\sigma_x - \sigma_y)^2 + (\sigma_y - \sigma_z)^2 + (\sigma_z - \sigma_x)^2 \ + 3(\tau^2_{xy} + \tau^2_{yz} + \tau^2_{zx})} \tag{2.20}$$

For plane strain deformation equation (2.19) and (2.20) reduce to

$$\dot{\bar{\epsilon}} = \frac{2}{3}\sqrt{3\,\dot{\epsilon}_x^2 + \frac{3}{4}\,\dot{\gamma}_{xy}^2} \tag{2.21}$$

since $\dot{\epsilon}_x = -\dot{\epsilon}_y$ and $\dot{\epsilon}_z = 0$

and

$$\bar{\sigma} = \sqrt{\frac{1}{4}(\sigma_x - \sigma_y)^2 + 3\tau_x^2} \tag{2.22}$$

since $$\sigma_z = \frac{\sigma_x + \sigma_y}{2}$$

Substituting (2.21) and (2.22) in (2.18) and the result into (2.17) yields

$$\dot{\epsilon}_x = \frac{3}{2}\,\frac{\dot{\bar{\epsilon}}}{\bar{\sigma}}\,(\sigma_x + p) \tag{2.23}$$

$$\dot{\epsilon}_y = \frac{3}{2}\,\frac{\dot{\bar{\epsilon}}}{\bar{\sigma}}\,(\sigma_y + p) \tag{2.24}$$

$$\dot{\gamma}_{xy} = 3\,\frac{\dot{\bar{\epsilon}}}{\bar{\sigma}}\,(\tau_{xy}) \tag{2.25}$$

where the hydrostatic stress (p) is

$$p = -\frac{1}{3}(\sigma_x + \sigma_y + \sigma_z)$$

Eleminating p in equations (2.23) and (2.24) gives

$$(\dot{\epsilon}_x - \dot{\epsilon}_y) = \frac{3}{2}\,\frac{\dot{\bar{\epsilon}}}{\bar{\sigma}}\,(\sigma_x - \sigma_y) \tag{2.26}$$

and solving for σ_x yields

$$\sigma_x = \sigma_y + \frac{2}{3}\,\bar{\sigma}\,\left(\frac{\dot{\epsilon}_x + \dot{\epsilon}_y}{\dot{\bar{\epsilon}}}\right) \tag{2.27}$$

Differentiating with respect to y, equation (2.27) yields

$$\frac{\partial \sigma_x}{\partial y} = \frac{\partial \sigma_y}{\partial y} + \frac{2}{3}\,\frac{\partial}{\partial y}\left(\frac{\dot{\epsilon}_x - \dot{\epsilon}_y}{\dot{\bar{\epsilon}}/\bar{\sigma}}\right) \tag{2.28}$$

Differentiation of equation (2.25) with respect to x yields

$$\frac{\partial \tau_{xy}}{\partial x} = \frac{1}{3} \frac{\partial}{\partial x} \left(\frac{\dot{\gamma}_{xy}}{\dot{\bar{\epsilon}}/\bar{\sigma}} \right) \tag{2.29}$$

Substituting equation (2.29) in equation (2.7) gives

$$\frac{\partial \sigma_y}{\partial y} = - \frac{\partial \tau_{xy}}{\partial x} = - \frac{1}{3} \frac{\partial}{\partial x} \left(\frac{\dot{\gamma}_{xy}}{\dot{\bar{\epsilon}}/\bar{\sigma}} \right) \tag{2.30}$$

substitution of equation (2.30) into (2.28) yields

$$\frac{\partial \sigma_x}{\partial y} = \frac{2}{3} \left[\frac{\partial}{\partial y} \left(\frac{\dot{\epsilon}_x - \dot{\epsilon}_y}{\dot{\bar{\epsilon}}/\bar{\sigma}} \right) - \frac{1}{2} \frac{\partial}{\partial x} \left(\frac{\dot{\gamma}_{xy}}{\dot{\bar{\epsilon}}/\bar{\sigma}} \right) \right] \tag{2.31}$$

The right hand side of equation (2.31) can be evaluated for any point in the flow field for which the strain rates have been determined and for which $\bar{\sigma}$ is known. Integration of equation (2.31) yields

$$\sigma_x = \frac{2}{3} \int_{y_1}^{y} \left[\frac{\partial}{\partial y} \left(\frac{\dot{\epsilon}_x - \dot{\epsilon}_y}{\dot{\bar{\epsilon}}/\bar{\sigma}} \right) - \frac{1}{2} \frac{\partial}{\partial x} \left(\frac{\dot{\gamma}_{xy}}{\dot{\bar{\epsilon}}/\bar{\sigma}} \right) \right] dy + K(x) \tag{2.32}$$

This equation was first derived in this form by Thomsen and Lapsley [3]. In equation (2.21), K(x) is given by

$$K(x) = [\sigma_x]_{y=y_1} \tag{2.33}$$

Boundary Conditions :

If σ_x is known at a point (x_1, y_1) in the plastic zone K(x) can be determined as follows :

$$\frac{\partial \sigma_x}{\partial x} = \frac{2}{3}\frac{\partial}{\partial x}\left[\left\{\int_{y_1}^{y}\frac{\partial}{\partial y}\left(\frac{\dot{\epsilon}_x - \dot{\epsilon}_y}{\dot{\bar{\epsilon}}/\bar{\sigma}}\right) - \frac{1}{2}\frac{\partial}{\partial x}\left(\frac{\dot{\gamma}_{xy}}{\dot{\bar{\epsilon}}/\bar{\sigma}}\right)\right\}dy\right] + \frac{dK}{dx} \qquad (2.34)$$

Differentiating equation (2.25) with respect to y gives

$$\frac{\partial \tau_{xy}}{\partial y} = \frac{1}{3}\frac{\partial}{\partial y}\left(\frac{\dot{\gamma}_{xy}}{\dot{\bar{\epsilon}}/\bar{\sigma}}\right) \qquad (2.35)$$

Substituting $\frac{\partial \tau_{xy}}{\partial y}$ from (2.35) into (2.6) yields

$$\frac{\partial \sigma_x}{\partial x} = -\frac{\partial \tau_{xy}}{\partial y} = -\frac{1}{3}\frac{\partial}{\partial y}\left(\frac{\dot{\gamma}_{xy}}{\dot{\bar{\epsilon}}/\bar{\sigma}}\right) \qquad (2.36)$$

Substituting $\frac{\partial \sigma_x}{\partial x}$ from (2.36) into (2.34) gives

$$\frac{2}{3}\frac{\partial}{\partial x}\left[\int_{y_1}^{y}\left\{\frac{\partial}{\partial y}\left(\frac{\dot{\epsilon}_x - \dot{\epsilon}_y}{\dot{\bar{\epsilon}}/\bar{\sigma}}\right) - \frac{1}{2}\frac{\partial}{\partial x}\left(\frac{\dot{\gamma}_{xy}}{\dot{\bar{\epsilon}}/\bar{\sigma}}\right)\right\}dy\right]$$

$$+ \frac{dK}{dx} + \frac{1}{3}\frac{\partial}{\partial y}\left(\frac{\dot{\gamma}_{xy}}{\dot{\bar{\epsilon}}/\bar{\sigma}}\right) = 0 \qquad (2.37)$$

Substituting $y = y_1$ in equation (2.37) yields

$$\left.\frac{dK}{dx}\right|_{y=y_1} + \frac{1}{3}\frac{\partial}{\partial y}\left.\left(\frac{\dot{\gamma}_{xy}}{\dot{\bar{\epsilon}}/\bar{\sigma}}\right)\right|_{y=y_1} = 0 \qquad (2.38)$$

Integration of equation (2.38) yields

$$K(x) = -\frac{1}{3}\int_{x_1}^{x}\left[\frac{\partial}{\partial y}\left(\frac{\dot{\gamma}_{xy}}{\dot{\bar{\epsilon}}/\bar{\sigma}}\right)\right]_{y=y_1} dx + \sigma_{x_o} \qquad (2.39)$$

where

$$\sigma_{x_o} = \sigma_x\Big|_{\substack{x = x_1 \\ y = y_1}} \qquad (2.40)$$

Substituting K(x) from equation (2.39) into equation (2.32) gives

$$\sigma_x(x,y) = \frac{2}{3}\int_{y_1}^{y}\left[\frac{\partial}{\partial y}\left(\frac{\dot{\epsilon}_x - \dot{\epsilon}_y}{\dot{\bar{\epsilon}}/\bar{\sigma}}\right) - \frac{1}{2}\frac{\partial}{\partial x}\left(\frac{\dot{\gamma}_{xy}}{\dot{\bar{\epsilon}}/\bar{\sigma}}\right)\right] dy$$

$$- \frac{1}{3}\int_{x_1}^{x}\left[\frac{\partial}{\partial y}\left(\frac{\dot{\gamma}_{xy}}{\dot{\bar{\epsilon}}/\bar{\sigma}}\right)\right]_{y=y_1} dx + \sigma_{x_o} \qquad (2.41)$$

The other normal stress component σ_y is obtained by substituting σ_x from equation (2.41) into equation (2.27)

$$\sigma_y(x,y) = \sigma_x - \frac{2}{3}\left(\frac{\dot{\epsilon}_x - \dot{\epsilon}_y}{\dot{\bar{\epsilon}}/\bar{\sigma}}\right) \qquad (2.42)$$

The shear stress component τ_{xy} is obtained from equation (2.25), i.e.

$$\tau_{xy} = \frac{1}{3}\left(\frac{\dot{\gamma}_{xy}}{\dot{\bar{\epsilon}}/\bar{\sigma}}\right) \qquad (2.43)$$

It is seen from equations (2.41), (2.42) and (2.43) that the stress field in the plastic zone is established, provided

(a) the strain rate field throughout the plastic zone is known,

(b) the effective stress $\bar{\sigma}$ is known throughout the field, and

(c) normal stress component is known in the plastic zone at one point.

When the velocity field is known, strain, rate field can be obtained from the following relations :

$$\dot{\epsilon}_x = \frac{\partial u_x}{\partial x} \qquad (2.44)$$

$$\dot{\epsilon}_y = \frac{\partial u_y}{\partial y} \qquad (2.45)$$

$$\dot{\gamma}_{xy} = \frac{\partial u_x}{\partial y} + \frac{\partial u_y}{\partial x} \qquad (2.46)$$

where u_x and u_y are X and Y components of velocity for any arbitrarily chosen cartesian coordinate axes (x,y).

The problem at hand cannot be dealt with easily in the cartesian coordinate system as the stress distribution in this case has an axial symmetry as shown in Fig. (2.1) with stress on the centre line at point 'A' as zero. The strain rates to be determined here are $\dot{\epsilon}_z$, $\dot{\epsilon}_\theta$, $\dot{\epsilon}_r$ and $\dot{\gamma}_{zr}$. The hoop strain rate $\dot{\epsilon}_\theta$ can be obtained from the volume contancy relationship as $\dot{\epsilon}_z$ and $\dot{\epsilon}_r$ are known. If we call the radial direction as r, then $\sigma_y = \sigma_r = 0$ at the point A r = 0.

To make the problem of axial symmetry analogous to that of plane, strain, the following simple substitution are to be made in equation (2.44), (2.45) and (2.46) :

$$\dot{\epsilon}_x \rightarrow \dot{\epsilon}_z \ , \tag{2.47}$$

$$\dot{\epsilon}_y \rightarrow \dot{\epsilon}_r \tag{2.48}$$

$$\dot{\gamma}_{xy} \rightarrow \dot{\gamma}_{zr} \tag{2.49}$$

By making these substitutions, equation (2.41) becomes

$$\sigma_z = \frac{2}{3} \int_{r_1}^{r} \left[\frac{\partial}{\partial r} \left(\frac{\dot{\epsilon}_z - \dot{\epsilon}_r}{\dot{\bar{\epsilon}}/\bar{\sigma}} \right) - \left(\frac{\dot{\epsilon}_r - \dot{\epsilon}_\theta}{r\dot{\bar{\epsilon}}/\bar{\sigma}} \right) - \frac{1}{2} \frac{\partial}{\partial z} \left(\frac{\dot{\gamma}_{zr}}{\dot{\bar{\epsilon}}/\bar{\sigma}} \right) \right] dr$$

$$- \frac{1}{3} \int_{z_o}^{z} \left[\frac{\partial}{\partial r} \left(\frac{\dot{\gamma}_{zr}}{\dot{\bar{\epsilon}}/\bar{\sigma}} \right) + \frac{\dot{\gamma}_{zr}}{r(\dot{\bar{\epsilon}}/\bar{\sigma})} \right]_{r=r_1} dz + \sigma_{z\theta} \tag{2.50}$$

where $\sigma_{z\theta} = [\sigma_z]_{r=r_1}^{z=z_o}$, is known.

Effective stress $\bar{\sigma}$ can be found from material tests. Thus it is seen that stress field is obtained once the velocity field is established.

2.2 FLOW FUNCTION METHODS

This method was developed by Shabaik and Thomsen [4] for analysing extrusion problems by visioplasticity technique.

In the present work, lines were drawn on the dimetral plane parallel to the length of the rod (along the z-axis as considered in the cylindrical coordinate system) which was also the direction of the drawing velocity.

Flow function ϕ' for any flow line is defined as volume flow rate per unit width of the workpiece between that flow line and a datum flow line. Considering the problem in cartesian coordinate system, for ease in establishing the theory.

$$\phi' = \int_{y_1}^{y_2} u_x \, dy \qquad (2.51)$$

Since the flow is steady (that is time invariant), from volume constancy conditions, flow function is constant along a flow line that is $d\phi' = 0$. In the steady state is only a function of x and y, therefore, the differential $d\phi'$ is given by

$$d\phi' = \frac{\partial \phi'}{\partial x} dx + \frac{\partial \phi'}{\partial y} dy = 0 \qquad (2.52)$$

Also at any point along flow line

$$\frac{dy}{dx} = \frac{u_y}{u_x} \tag{2.53}$$

Substituting equation (2.53) in equation (2.52) yields

$$\frac{\partial \phi'}{\partial x} u_x + \frac{\partial \phi'}{\partial y} u_y = 0 \tag{2.54}$$

Differentiation of (2.51) yields

$$u_x = \frac{\partial \phi'}{\partial y} \tag{2.55}$$

Substituting equation (2.55) in equation (2.54) yields

$$\frac{\partial \phi'}{\partial x} \cdot \frac{\partial \phi'}{\partial y} + \frac{\partial \phi'}{\partial y} u_y = 0 \tag{2.56}$$

Therefore,

$$u_y = - \frac{\partial \phi'}{\partial x} \tag{2.57}$$

With reference to the flow line passing through the centre of the cylindrical rod (Fig. 2.2), flow function along any flow line is given by

$$\phi' = t_o \, v_o \tag{2.58}$$

where t_o is the initial spacing up stream from the reference flow line and V_o is the drawing velocity.

From equation (2.42), ϕ' is obtained for each flow line. Velocity field can then be obtained using the relations (2.55) and (2.57).

Flow function method has two inherent advantages.

a) It presumes volume constancy condition. This excludes the need to modify the strain rate field so that it satisfies

equation (2.15), b) only one set of parallel lines need be scribed. In other methods usually two sets of perpendicular lines have to be scribed.

For the sake of completeness, few other methods for establishing velocity field are discussed.

2.3 SOME OTHER METHODS FOR ESTABLISHING VELOCITY FIELD

(a) Method of Incremental deformation :

Thomsen and Lapsley [3] used a split lead billet for extrusion with square grid inscribed on the meridian plane. After each incremental deformation the billet was opened and the deformation was recorded. Later by superimposing the successive grid patterns, they obtained the velocity field.

(b) Palmer and Oxley's method :

Palmer and Oxley [5] used cine' film to record paths of the individual grains on the side of a machined workpiece. Stream lines (or flow lines) were plotted by tracing the paths of a number of particles as they moved through the deformation zone. The inherent disadvantage of this method is that it results in a flow pattern, the different parts of which refer to different instant of time.

(c) Zorev's method:

Zorev [6] obtained steady state pattern of a grid originally square with abscissae parallel to the cutting speed V_o Fig. 2.3.

He further assumed that the average absolute velocity between any two network nodes 1 and 2 along the same flow line is given by

$$V = V_o \frac{a}{a_o} \tag{2.59}$$

where a_o and a are undeformed and deformed grid spacings.

The X and Y components of velocity are then given by

$$u_x = \frac{V_o}{a_o} a \cos \alpha \tag{2.60}$$

$$u_y = \frac{V_a}{a_o} a \sin \alpha \tag{2.61}$$

where α is the angle made by the tangent to a_o a flow line with X-axis.

Differentiation of equation (2.60) and (2.61) with respect to x and y respectively yields the strain rate components.

$$\dot{\epsilon}_x = \frac{\partial u_x}{\partial x} = \frac{V_o}{a_o} \left[\frac{\partial a}{\partial x} \cos \alpha - a \sin \alpha \frac{\partial \alpha}{\partial x} \right] \tag{2.62}$$

$$\dot{\epsilon}_y = \frac{\partial u_y}{\partial y} = \frac{V_o}{a_o} \left[\frac{\partial a}{\partial y} \sin \alpha + a \cos \alpha \frac{\partial \alpha}{\partial y} \right] \tag{2.63}$$

$$\dot{\gamma}_{xy} = \frac{\partial u_x}{\partial y} + \frac{\partial u_y}{\partial x}$$

$$= \frac{V_o}{a_o} \left[\sin \alpha \left(\frac{\partial a}{\partial x} - \frac{a \partial \alpha}{\partial y} \right) + \cos \alpha \left(\frac{\partial a}{\partial y} + a \frac{\partial \alpha}{\partial x} \right) \right] \tag{2.64}$$

This technique gives fairly accurate results if the original grid spacings are sufficiently narrow.

(d) Das, Ghosh and Ghosh's Method :

Das, Ghosh and Ghosh [7] employed a variation of Zorev's method for a case of axisymmetric extrusion. They assumed a linear velocity variation between consecutive network nodes along a flow line.

Let S (Fig. 2.4) be the original grid spacing and V be the billet velocity. Also let S_{22} be spacing between two nodes 22 and 32 in the steady state deformation pattern. It is assumed that velocity upto node 22 is already computed. The average velocity of the material particle while moving from 22 to 32 is given by

$$V_{22av} = V.(S_{22}/S) \tag{2.65}$$

which is the same as equation (2.59). Since the velocity between two nodes is assumed to vary linearly, the velocity at a distance x from node 22 along flow line is given by

$$\frac{dx}{dt} = V_{22} + \frac{x}{S_{22}} \Delta V_{22} \tag{2.66}$$

where $\Delta V_{22} = V_{32} - V_{22}$ (2.67)

Integration of equation (2.66) yields

$$\frac{dx}{V_{22} + \frac{\Delta V_{22}}{S_{22}}. x} = t + C \tag{2.68}$$

where C is the constant of integration

or

$$\frac{S_{22}}{\Delta V_{22}} . \ell n\ V_{22} + \frac{\Delta V_{22}}{S_{22}} . x = t + c \qquad (2.69)$$

Choosing $x = 0$, at $t = 0$, yields, from equation (2.69)

$$t = \frac{S_{22}}{\Delta V_{22}} . \ell n \left[1 + \frac{\Delta V_{22}}{V_{22}} \right] \qquad (2.70)$$

Thus the time t_{22} required for a particle to travel from node 22 to node 32 is given by

$$t_{22} = \frac{S_{22}}{\Delta V_{22}} . \ell n \left[1 + \frac{\Delta V_{22}}{V_{22}} \right] \qquad (2.71)$$

Average velocity, therefore, between nodes 22 and 32 is

$$V_{22av} = \frac{S_{22}}{t_{22}} = \frac{S_{22}\ \Delta V_{22}}{S_{22} . \ell n \left[1 + \frac{\Delta V_{22}}{V_{22}} \right]} \qquad (2.72)$$

Comparison of equation (2.65) and (2.72) yields

$$\frac{VS_{22}}{S} = \frac{\Delta V_{22}}{\ell n \left[1 + \frac{\Delta V_{22}}{V_{22}} \right]} \qquad (2.73)$$

Let $\Delta V_{22}/V_{22} = x$ and $\frac{V}{V_{22}} . \frac{S_{22}}{S} = C$ then equation (2.73) becomes

$$Y - C . \ell n\ (1 + x) = 0 \qquad (2.74)$$

Thus the velocity can be computed for each point by solving equation (2.74) by usual numerical methods. An extension of this process with modifications has been used in the present work as would be evident from the following chapters.

(e) Childs' method :

Childs [8] developed a noval method for obtaining velocity field in the deformation zone during orthogonal planing experiment. A grid of squares is inscribed on the side of the workpiece and while it is being deformed by a cutting tool, it is observed through a microscope, side flow is prevented by a toughned glass plate. Two photographs one taken a known time interval after the other, enables measurement of velocity from the displacement of the grid crossings. Both photographs are recorded on the same frame of the film, using dark field microscopy. The camera has no shutter. The guided spark flash guns have flash duration of 2.0×10^{-6} sec. which limits the maximum possible cutting speed to above 95 metres/min. (300 ft/min.).

The methods discussed so far for obtaining velocity field can only be applied to steady state processes. Work has also been done on unsteady process. One of the visioplasticity techniques for unsteady processes is due to Santos and Organ [9]. They have applied it for the deformation of ductile fracture process.

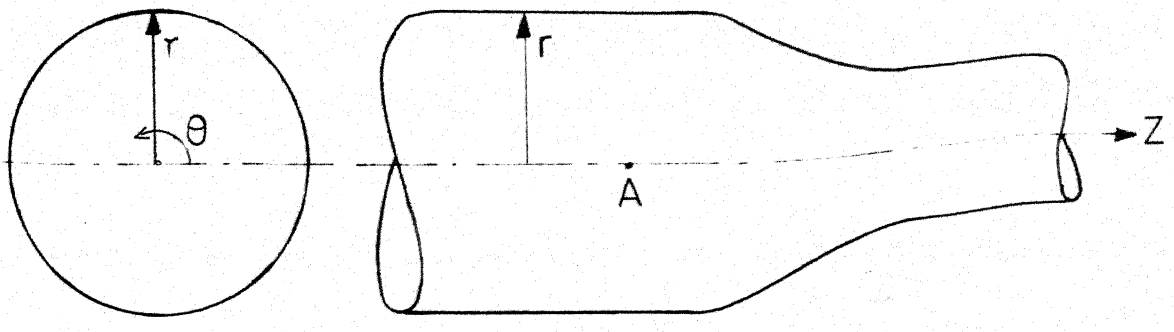

Fig. 2·1 Axial symmetry case

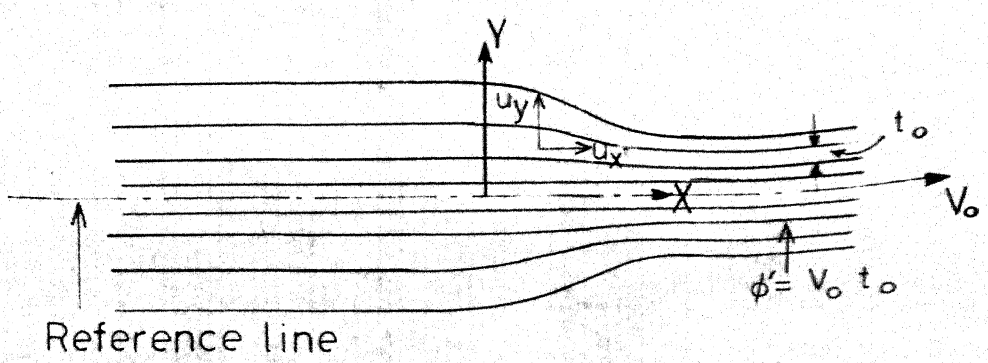

Fig. 2·2 Velocity distribution in axial symmetric billet

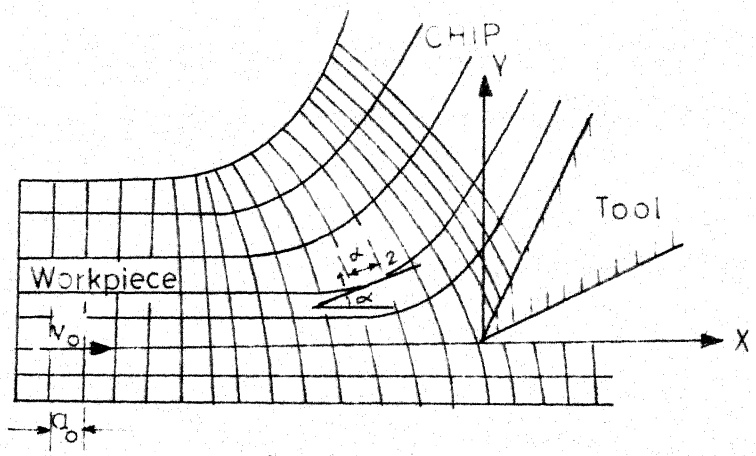

Fig. 2·3 Velocity distribution (Zorev's Method)

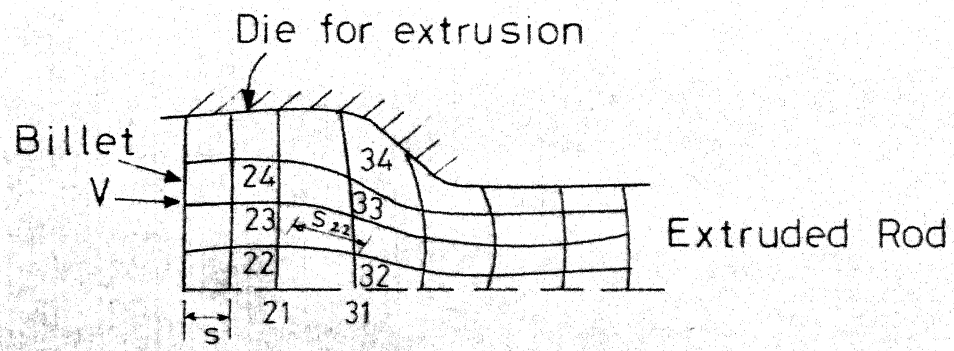

Fig. 2·4 Velocity distribution pattern in extruded billet (Das Ghosh & Ghosh)

C H A P T E R - 3

EXPERIMENTAL SET-UP

3.1 INTRODUCTION

The experimental set-up consisted essentially of two major portions. a) A rod drawing mechanism and b) a special type of dynamometer which could measure the drawing force and the separating force simultaneously and independent of each other.

At the on-set of experiment neither a rod drawing machine was available nor a suitable dynamometer existed which could measure the drawing and separating forces simultaneously. The experimental set-up was, therefore, designed on a straight bed model LB 17 HMT Lathe which had ten HP available for drawing purpose. The machine was set-up as a draw bench and a disc type dynamometer was specially designed for measuring the drawing and separating forces independently.

3.2 DESIGN OF A DISC TYPE DYNAMOMETER

A dynamometer is used in order to measure the instantaneous values of forces occurring while material is being drawn through a die. It is usually most convenient to measure these forces relative to a set of two or three-dimensional rectangular co-ordinates. The important requirements for any dynamometer are

a) High sensitivity

b) High rigidity

c) Linear relationship between magnitude of the force being measured and readings in the recorder, with no hysteresis phenomenon

d) No cross sensitivity amongst the various forces being measured

e) Stability relative to time temperature and humidity.

Several types of dynamometers satisfying the above requirements have been developed in various respect projects but none of these designs were suitable for the present work.

To measure both the drawing and the separating forces a two component dynamometer with semiconductor strain gauges was designed and fabricated. It consists of an elastic disc in the centre of which a 12 degrees taper hole is made to install a tapered split die with an outside taper of 12.5 degrees. The die fits in such a way that it remains exactly midway between the central boss.

The details of this disc dynamometer is shown in Figures 3.1(a) and (b). The main part of the dynamometer is an elastic disc which is supported at its periphery. A split die is installed on a circular boss in the centre of the disc. Twelve strain gauges are attached to the two surfaces of the disc as illustrated in the figure.

AA'BB' are the strain gauges for the measurement of the drawing force while CC'DD' measure the separating force.

Strain gauges EE'FF' are dummy gauges installed for the bridge formation for the separating force. This dynamometer is set before the drawing ram of a rod drawing machine with a suitable support to take the elastic load of drawing.

The principal of independently measuring the drawing and the separating forces is explained as follows.

The drawing force deforms the disc in a spherical form as shown in Fig. 3.2. To measure the separating force the thickness of the disc is reduced to 1/3 of the original over a small area i.e. small niches are made on either side of the disc by removing about 1/3rd of the metal from the surface equidistant from the centre and dimetrically opposite each other. The strain gauges are placed in these niches. By doing so the sensitivity of the niched area increases considerably as the magnitude of the separating force is small compared to the drawing force.

The two halves of the split die are positioned in a manner to face the strain gauges in the niches. When the die is loaded, the two halves produce a compressive force on the gauges which is then transmitted to the recorder.

The connection of the wires for the strain gauges and deflection of the disc during drawing are shown in Figures 3.4 and 3.5 which correspond to the measurement of the drawing force and separating force, respectively.

Strain gauges ABA'B', for the drawing force, are connected as shown in Fig. 3.4. According to the deflection of the disc, due to the pull caused by the drawing force, strain gauges A and B are put in compression and A'B' are put in tension. This causes an imbalance in the bridge and an output proportional to the magnitude of the drawing force flows through the recorder. Even if the separating force deforms the disc, strain gauges AA'BB' are subjected to the same magnitude of compression and the balance in the bridge is not affected.

As is evident from the Fig. 3.5, all four strain gauges would deflect in the same direction. Hence a pair of dummy gauges are mounted on the disc to obtain the difference between static and loaded conditions for the separating force as depicted by the bridge diagram of Fig. 3.5. There will be no effect of the drawing force on this bridge because compression caused in C and D will be nullified by the tension caused in C' and D', respectively and an output proportional to the magnitude of the separating force will flow through the bridge. Thus both the drawing force and the separating force could be measured independently.

The two forces can also be measured with only six strain gauges AB'CDE and F in place of the twelve strain gauges, but the sensitivity of the measurement will be reduced. The bridges are fully compensated for any change in resistence due to temperature because of the symmetrical connection of

the bridges. Further, this dynamometer involves no friction.

3.3 DEFORMATION OF DYNAMOMETER DISC :

The type of deformation of the disc dynamometer designed was analysed theoretically following the analysis proposed by Okushima and Hitomi [10] and the best position for attaching the strain gauges was determined from the theory of elasticity.

The disc dynamometer is shown schematically in Fig. 3.6. The diameter of the disc is denoted as $2r_1$ and the thickness of the disc is denoted as t. The periphery of the disc is supported rigidly. The split die is installed on a rigid circular boss of radius r_o in the centre of the disc.

Deflection due to drawing force

Drawing force P deforms the disc dynamometer as shown. Tensile or compressive strain at an arbitrary point on the surface of the disc, whose distance from the centre is r_1 is expressed as

$$\epsilon_{r_o} = \mp \frac{m^2-1}{m^2 E} \frac{3}{2\pi} \frac{P}{t^2} \left(\ell n\, r - \frac{r_o^2 r_1^2}{r_1^2 - r_o^2} \ell n \frac{r_1}{r_o} \cdot \frac{1}{r^2} + \frac{r_o^2 \ell n\, r_o - r_1^2 \ell n\, r_1}{r_1^2 - r_o^2} + 1 \right) \qquad (3.1)$$

where minus sign is for tensile strain at surface I and the plus sign is for compressive strain at surface II and E is Young's modulus of elasticity and m is Poisson's ratio.

Considering the tensile strain at surface I, the function of the strain is a decreasing function in respect to radius r, because

$$\frac{d\varepsilon_{r_o}}{dr} = \frac{-m^2-1}{m^2 E} \frac{3}{2\pi} \frac{P}{t^2} \left[\frac{1}{r} + \frac{r_o^2 r_1^2}{r_1^2 - r_o^2} \ell n \frac{r_1}{r_o} \cdot \frac{2}{r^3} \right] < 0 \qquad (3.2)$$

Therefore, the maximum value of the tensile or compressive strain on the surface of the disc exists at the edge of the rigid boss, namely at $r = r_o$, and is expressed as

$$\varepsilon_{r_o \max} = \pm \frac{m^2-1}{m^2 E} \frac{3}{2\pi} \frac{P}{t^2} \left[\frac{2r_1^2}{r_1^2 - r_o^2} \ell n \frac{r_1}{r_o} - 1 \right] \qquad (3.3)$$

where the plus sign is for maximum tensile strain at surface I and minus sign is for the maximum compressive strain at surface II.

When the disc is subjected to the drawing force, it is deformed as shown in Fig. 3.7. The deflection at an arbitrary point on the centre surface of the disc whose distance from the centre is r, is expressed as

$$w = \frac{m^2 - 1}{m^2 E} \frac{3}{2\pi} \frac{P}{t^3} \left[\left(\frac{r_o^2 \ell n r_o - r_1^2 \ell n r_1}{r_1^2 - r_o^2} - \frac{1}{2} \right) r^2 + r^2 \ell n r + \frac{2r_o^2 r_1^2}{r_1^2 - r_o^2} \ell n \frac{r_1}{r_o} \ell n r + \frac{r_1^2}{2} - \frac{r_o^2 r_1^2}{r_1^2 - r_o^2} (2 \ell n r_1 - 1) \ell n \frac{r_1}{r_o} \right] \qquad (3.4)$$

This deflection is a maximum at the edge of the boss. The equation for the maximum deflection of the disc due to the

drawing force is obtained from the above equation putting $r = r_o$. Hence,

$$w_{max} = \frac{m^2-1}{m^2 E} \frac{3}{4\pi} \frac{P}{t^3} \left[r_1^2 - r_o^2 - \frac{4r_o^2 r_1^2}{r_1^2 - r_o^2} (\ln \frac{r_1}{r_o})^2 \right] \qquad (3.5)$$

The separating force is unidirectional and is maximum along a radial line cutting the two halves of the split die at their mid points.

The best position for attaching the strain gauges is the periphery of the boss in the centre of the disc for the drawing force and the strain gauges for the separating force can be fitted anywhere on the disc after making the niches as discussed earlier.

3.4 CONSTRUCTION OF THE DYNAMOMETER

To construct the dynamometer a square plate of mild steel having the dimensions as 320 × 320 × 12.5 (thickness) mm. was taken. The point of intersection on its diagonals on its two faces were located, and two circles of radii 40 mm and 100 mm were marked on it. Metal was removed equally from both sides on a lathe till the thickness was reduced to 6 mm (Fig. 3.6). A 20 mm. tapered hole was made in the central boss at a taper angle of 12 degrees to hold a split die.

Semiconductor strain gauges were attached on to it as shown in Figures 3.4 and 3.5. For attaching strain gauges as shown in Fig. 3.5 metal was further removed equally from

both faces of the disc till niches only 2 mm thick were formed. The niches were made at r = 70 mm.

With the disc only 6 mm thick the maximum deflection of the central boss for 1 Kg. force was evaluated by equation (3.5) to be 0.6×10^{-6} mm. Since the material was mild steel. It was assumed that the poissons ratio m = $\frac{10}{3}$ and Young's modulus of elasticity E = 2,100,000 Kg./cm^2.

The plate of 320 mm square was welded on an angular support so that it may be held in a vertical position in front of the rod drawing ram. The plan of the supports for the dynamometer is shown in Fig. 3.8.

The sensitivity of a disc dynamometer of this type depends upon the diameter and thickness of the disc and the diameter of the rigid circular boss. The larger the diameter of the disc, and the smaller the thickness of the disc and the diameter of the boss, the more sensitive will be the dynamometer. However, in this manner, the deflection of the disc increases which in turn gives rise to second order interference in the strain gauges and the cross-sensivity between the channels increases. Keeping this in mind an optimum diameter and thickness are to be chosen. Since in the present work forces above 400 Kgs. were not be encountered, the above mentioned dimensions were chosen which gave a moderate deflection i.e.

$$\epsilon_{r_{o\ max}} \text{ at } r_o = 40 \text{ mm as } 0.6 \times 10^{-6} \text{ mm.}$$

3.5 DYNAMOMETER CALIBRATION

After the dynamometer was assembled and the strain gauges fitted as described, it was placed on four equally high supports at its four corners. The two bridges were connected to two channels of an Encardio-Rite recorder. Dead weights were placed on the central boss of the dynamometer in increasing steps of 10 Kgs. upto a maximum of 70 Kgs. and then removed in steps of 10 Kgs. This gave a plot for both loading and unloading of the central boss for the drawing force. The readings obtained in the other channel in this position gave the cross sensitivity error to be corrected from the readings of the separating force.

To calibrate for the separating force, a wire hook was put through the tapered hole of the dynamometer whose other end was firmly clamped through the hollow spindle. Another hook having a calibrated spring attached to it had one of its end fixed to the tapered hole of the central boss and the other end was clamped to the tool post. In this way known load could be applied just by moving the carriage of the lathe. Care was taken to pull the spring loaded hook in the direction of the line joining the two niches. This gave the separating force and the cross sensitivity due to this was read in the graph for drawing force.

The calibration curves for the drawing and separating forces are given in Figures 3.9 and 3.10. The curves in both the cases are linear and the cross-sensitivity between the two

was found to be less than 3 percent.

3.6 WIRE DRAWING MACHINE

A machine to draw a 12.5 mm thick wire was not available. An HMT lathe model LB 17 was modified to work as a draw bench. Details of this machine are given in Appendix A.

The tail stock bed was first fixed as near the chuck as the bed would permit. On this bed the dynamometer was bolted down so that it may be held there rigidly. A long clamp was made to hold the end of the wire (rod) on the smaller side of the die. This clamp was held on the total post on the carriage of the machine. The rod was fed through the hollow spindle.

Once the rod was held in the clamp and the carriage given an auto feed the rod could be drawn while the two forces could be recorded. Knowing the gear combination used the velocity at which the wire was being drawn was known.

3.7 WORK MATERIAL

Lead was used as the rod material since it closely approximates rigid plastic material behaviour. A stress-strain curve from the compression test of work material and its rigid plastic idealization is shown in Fig. 3.9.

It was required to have the rod cut exactly through the diameter. To overcome this problem, two strips 12.5 mm × 6.25 mm × 300 mm wire taken. By combining these together a square of 12.5 mm × 12.5 mm × 300 mm was obtained, corners of which were

rounded off to obtain a rod of 12.5 mm dia split at the diameter.

The two flat faces were smoothed first with fine emery paper and then polished with 200 mesh alumina powder soaked in oil and applied by a leather piece. The next requirement was to inscribe 10 to 12 lines on the 12.5 mm flat face on one of the interfaces.

Various methods of producing grid lines by mechanical and photographic means have been summerised by Baraya [11]. Square grids can be drawn using a chaser, which consists of a half cylinder on which very sharp threads are cut and hardened. It is suggested that a better method is to use a milling cutter with threads on its surface. This can be used to produce upto 45 lines per cm. A sharp cutting tool fitted to a universal measuring machine can give grids having 125 lines per centimetre (300 lines per inch). Lines have been drawn 0.025 mm (.001 in.) apart, using a Vickers microhardness testing machine, with a micrometer controlled stage beneath it.

Photolithography can successfully be used to generate square grids (upto 100 lines per centimetre). It can be used to obtain grids if any other geometry should an experiment demand so.

For the present work, since 10 to 12 lines per centimetre were deemed sufficient for the study at hand, a high speed steel hacksaw blade, having 12 teeth per centimetre was

held on the arbor of a horizontal milling machine with a special clamping arrangement devised for this purpose. One of the polished halves was rigidly held in a 300 mm long mild steel semicircular support on the table. The table was raised till the sharpened and pointed teeth dug slightly into the metal. The table was then transversed which resulted in marking fine even lines on the workpiece. The workpiece was again polished with alumina powder to ensure that any side flow that may have occurred, during the line scratching are removed. This method gave workpieces with 12 fine uniform lines neatly inscribed on one of the interface.

3.8 SPLIT DIE

To draw this lead rod a special split die of high carbon steel was made having a die angle (half cone angle) of 3 degrees. This would result in a reduction of 10 per cent in diameter as the effective width of the die was kept equal to 12.5 mm. This was also confirmed from experimentally measured values. If calculated on the basis of area the reduction would work out to be 19.86 per cent (approximately 20 per cent).

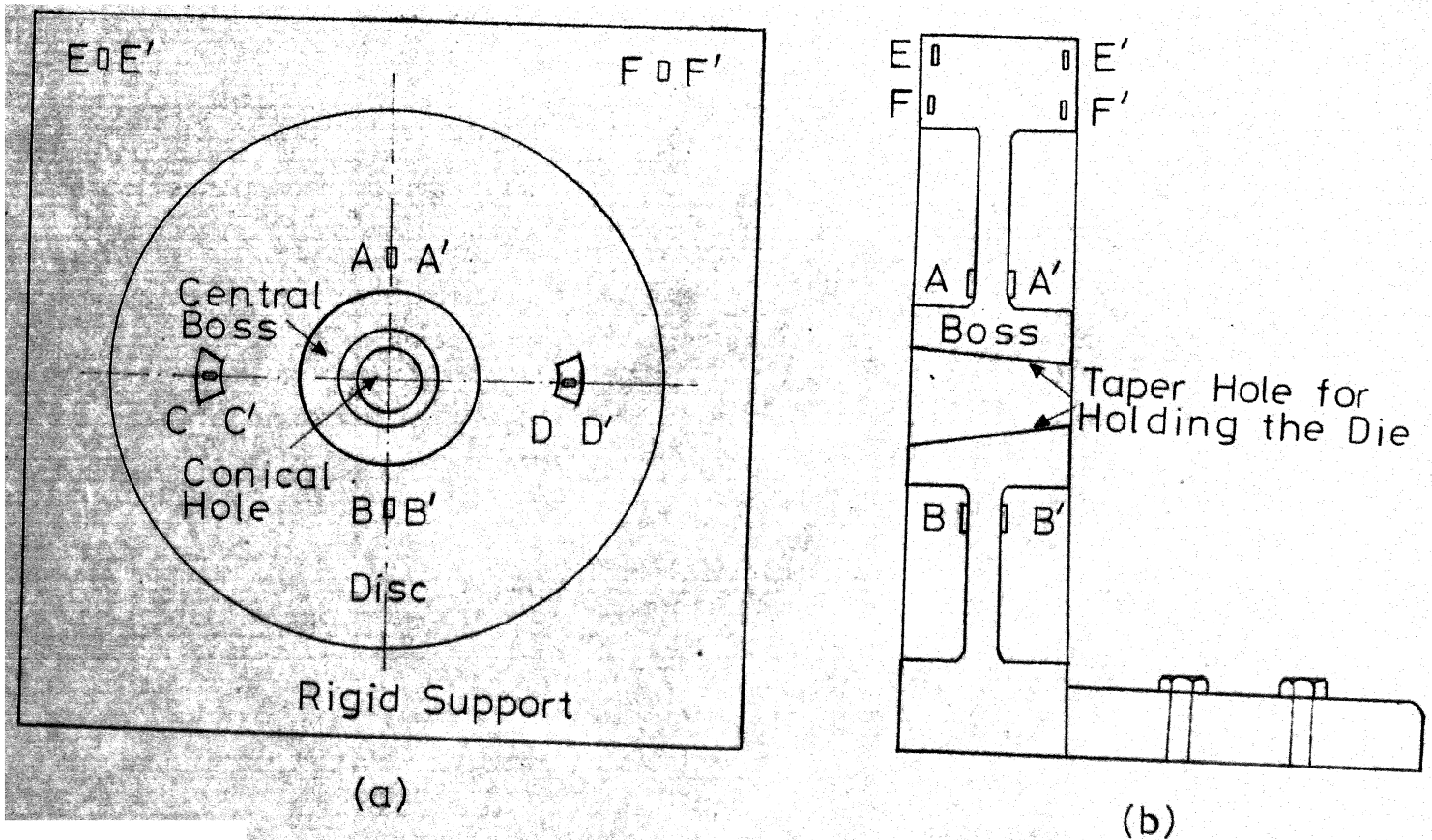

Fig.3·1 Details of the disc dynamometer

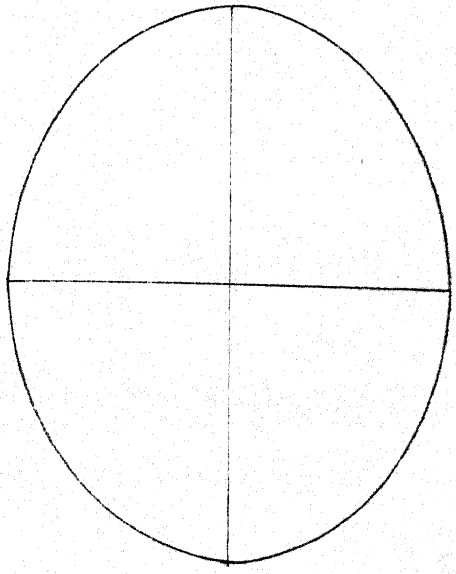

(a)

Undeflected disc dynamometer

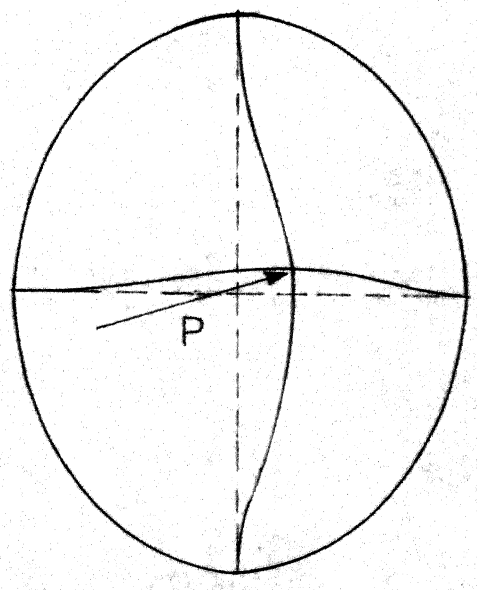

(b)

Deflection of disc dynamometer due to drawing force

Fig. 3·2

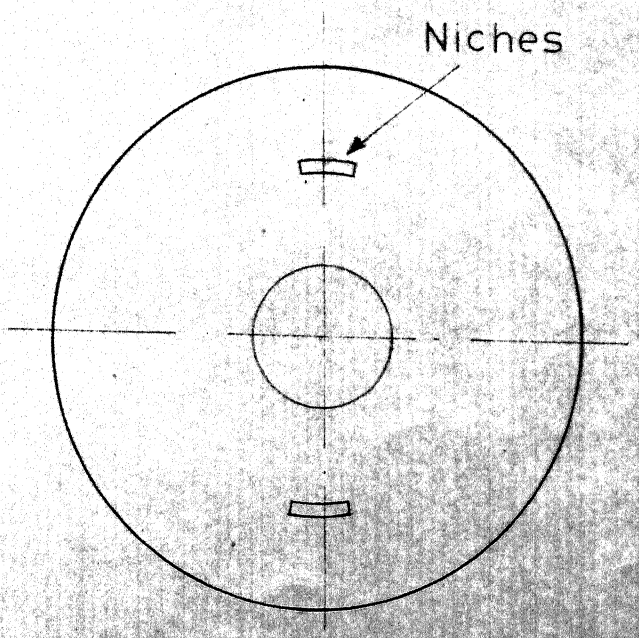

(a)

Undeformed disc geometry

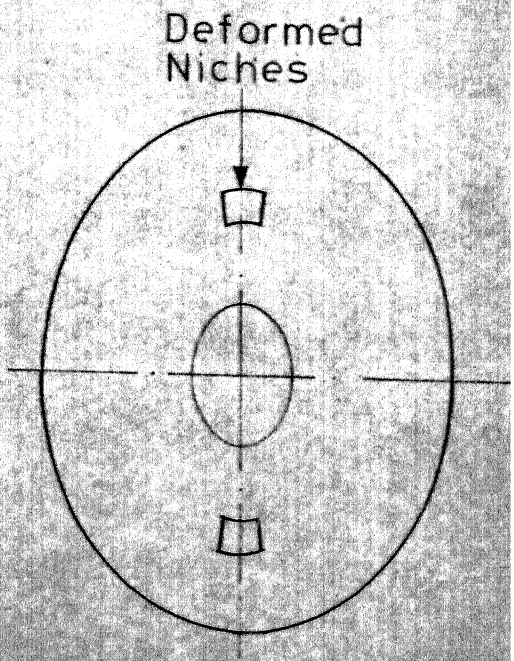

(b)

Deformed geometry of the disc due to separating force

Fig. 3·3

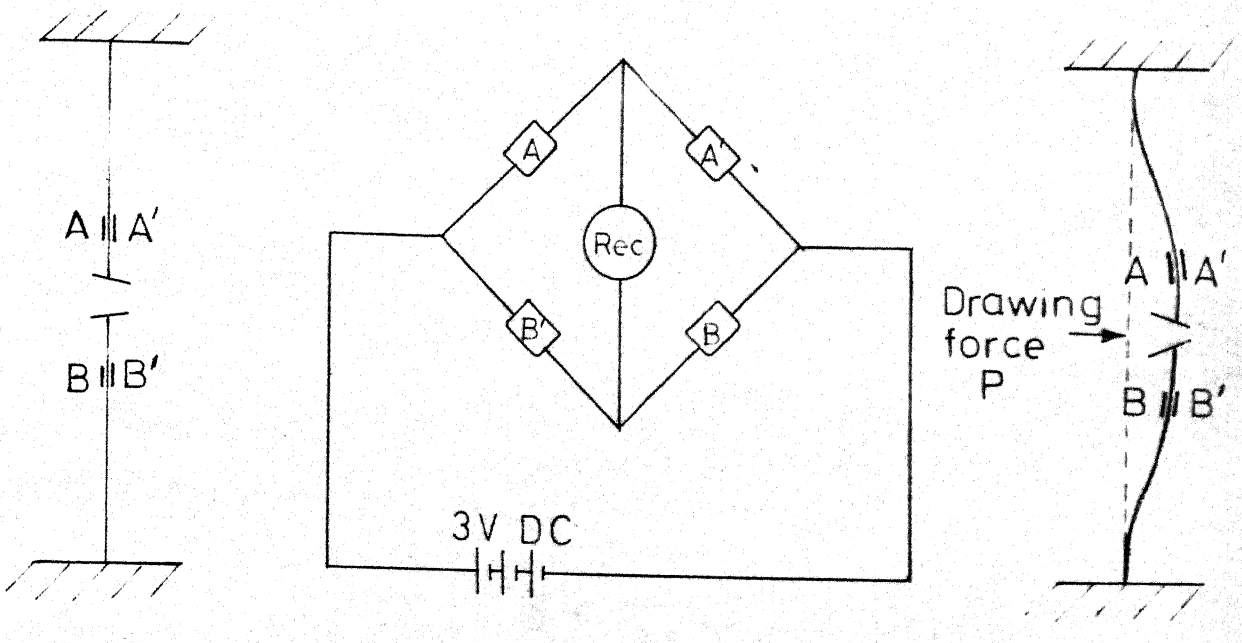

Fig. 3·4 Connection and operation of the strain gauges for the drawing force

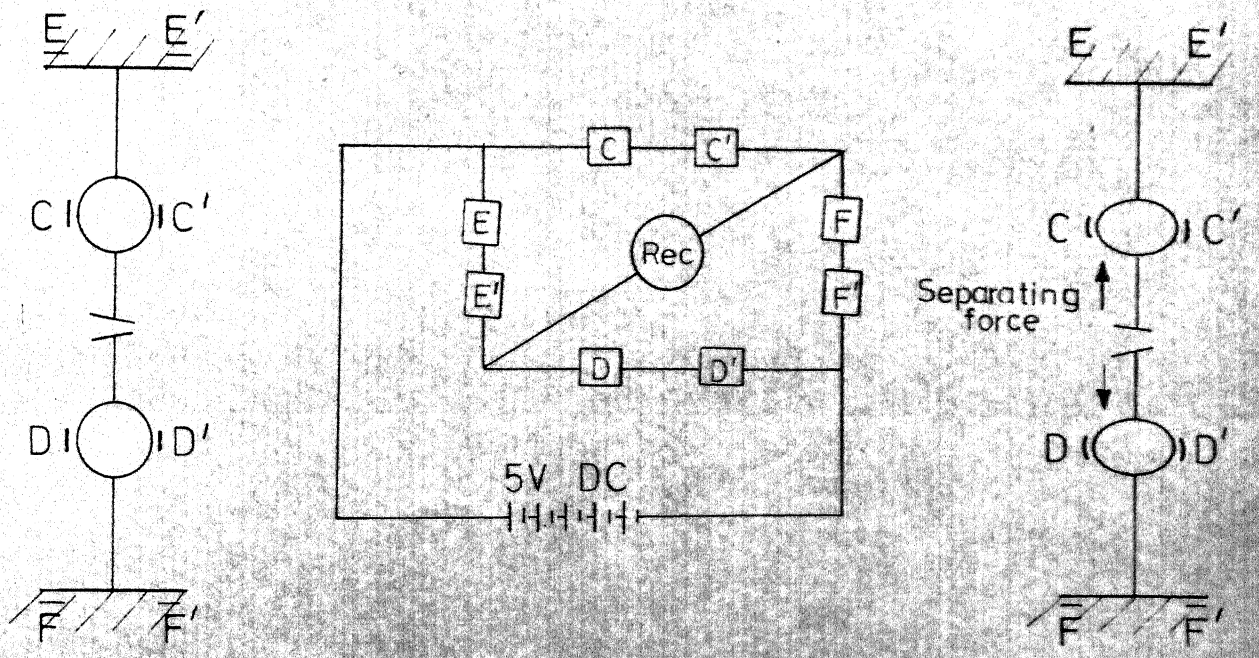

Fig. 3·5 Connection and operation of the strain gauges for the separating force

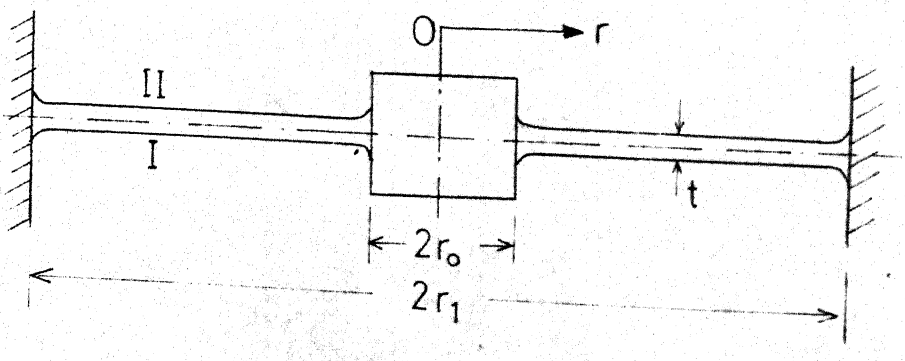

Fig. 3·6 Schematic view of the disc dynamometer designed

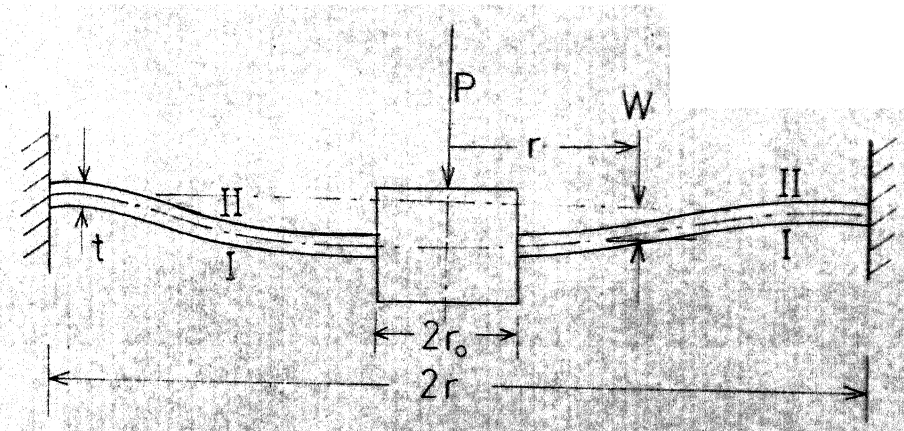

Fig. 3·7 Schematic view of deflection of the disc dynamometer due to the drawing force

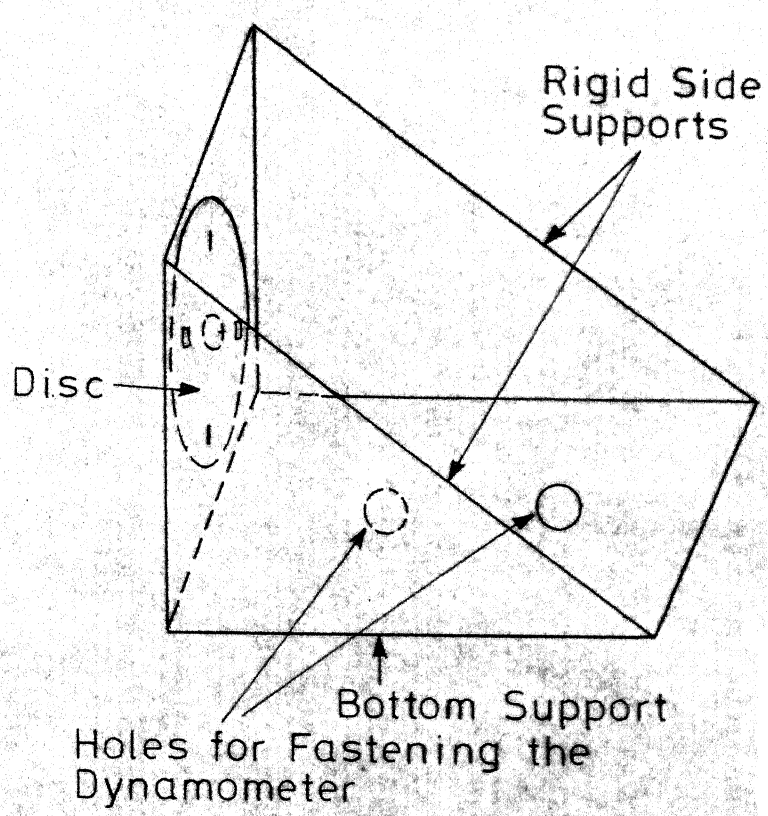

Fig. 3·8 Schematic view of the disc dynamometer

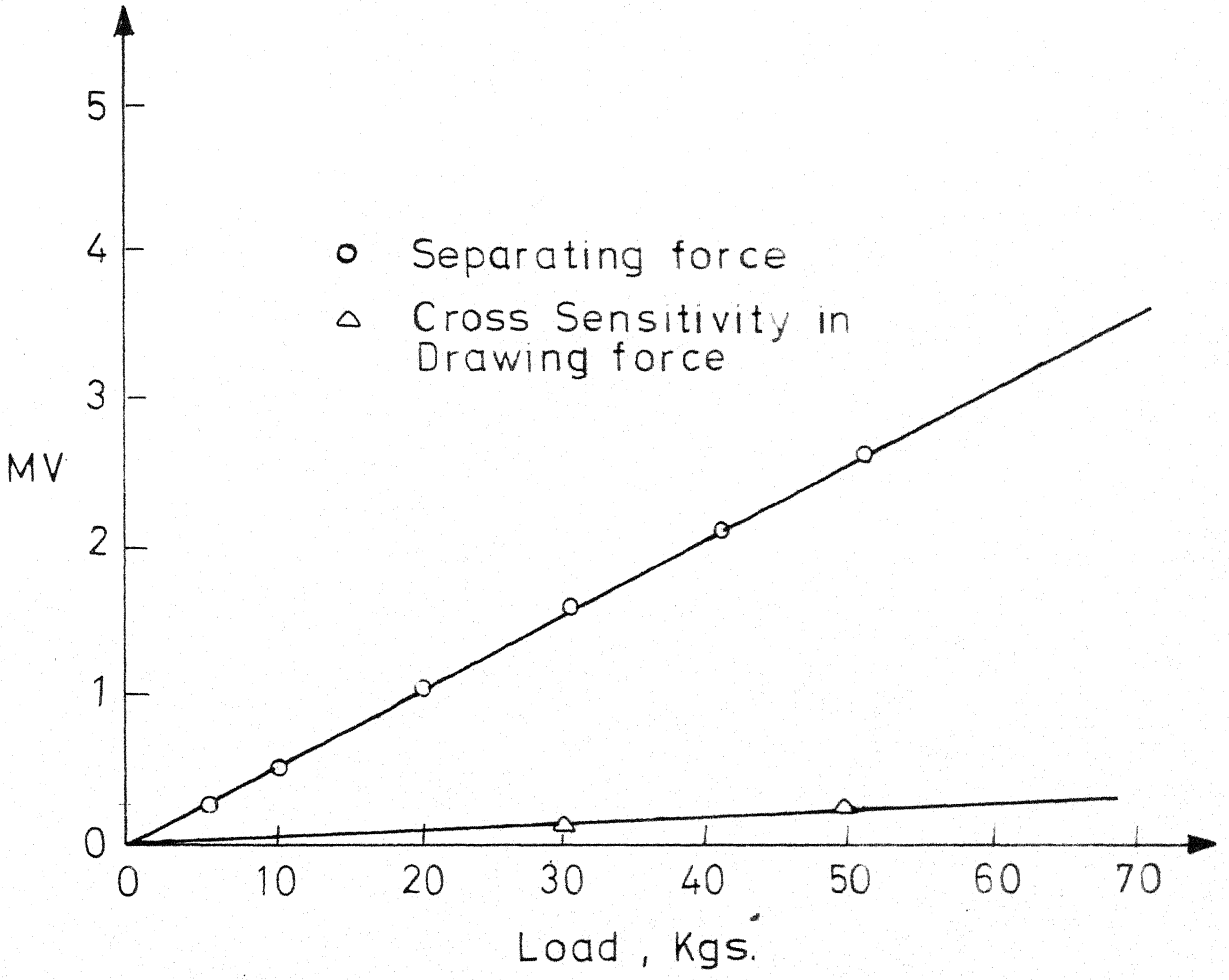

Fig. 3·10 Calibration curve of the disc dynamomete for Separating force

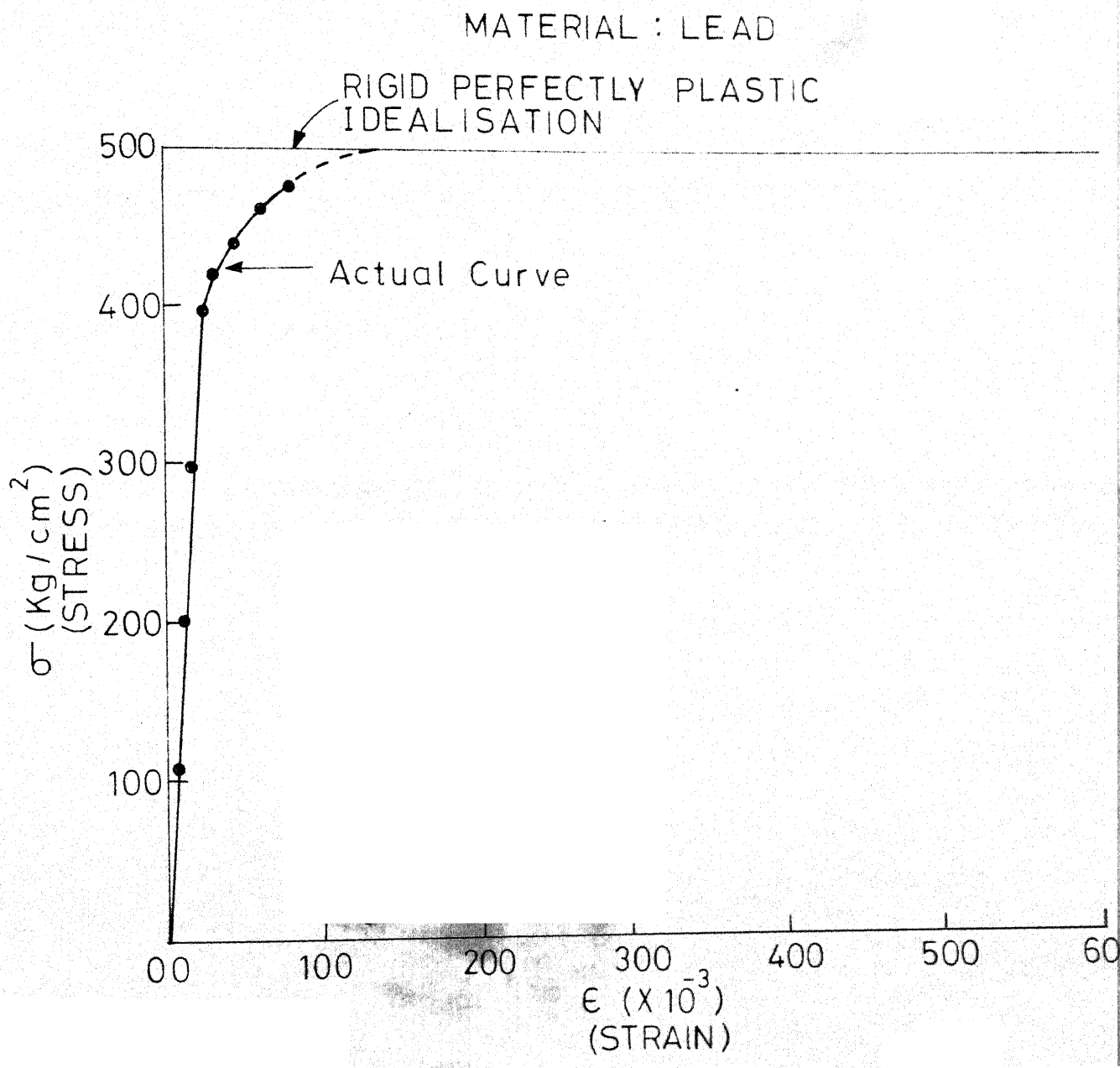

Fig. 3·11 Static stress strain curve from compression test

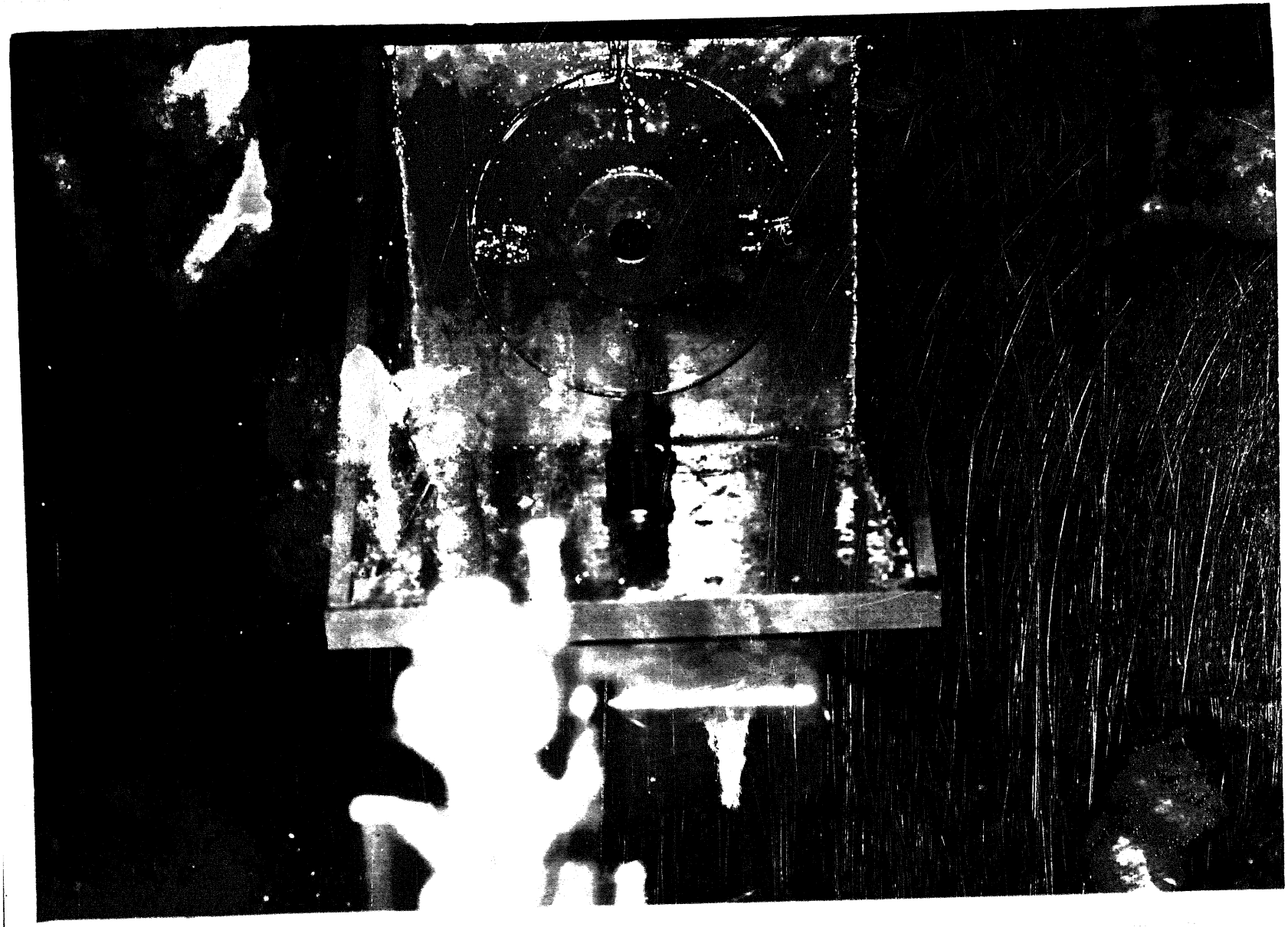

FIG. 3·12 THE DISC DYNAMOMETER

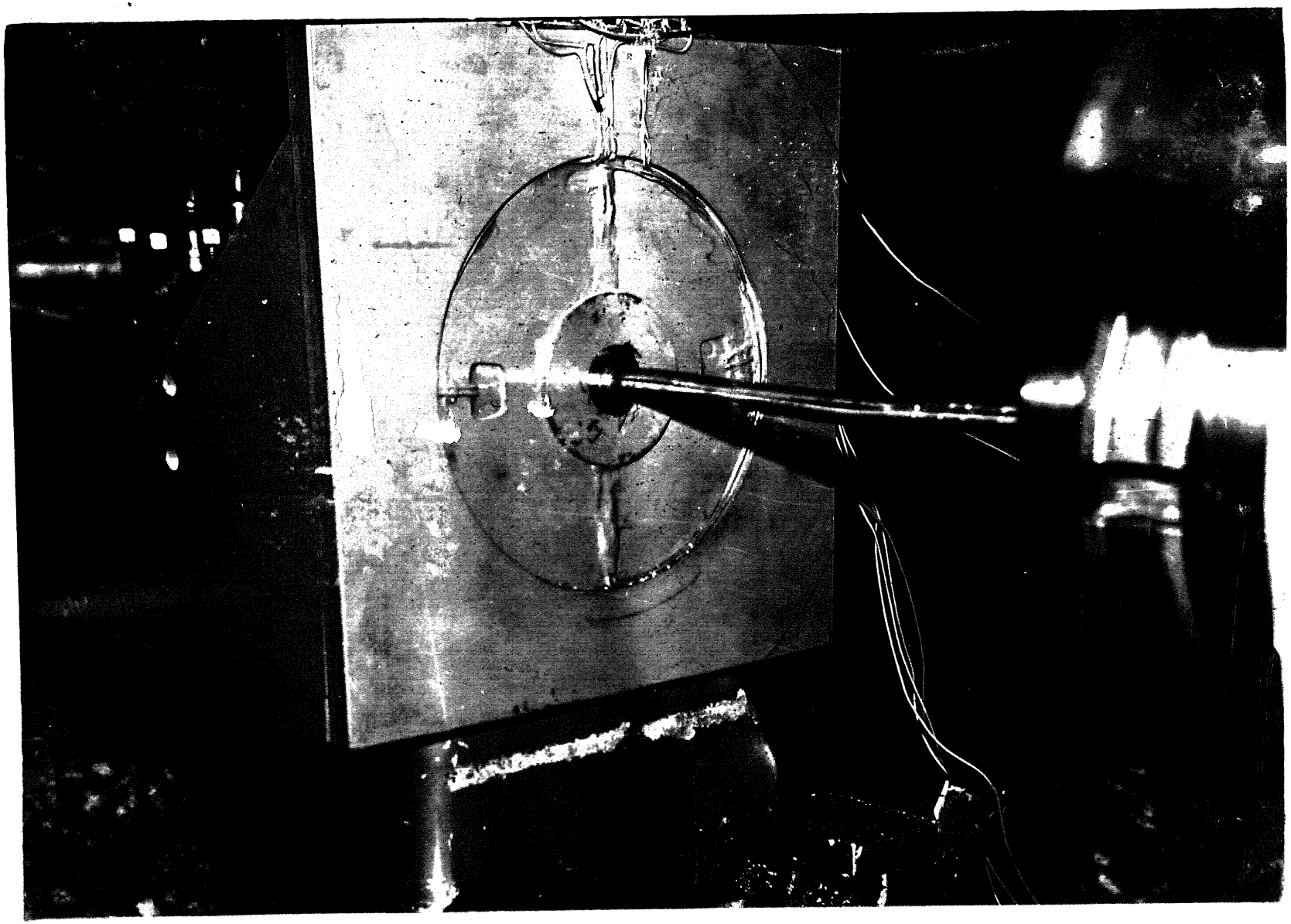

FIG.3·13 THE DYNAMOMETER SET UP ON THE DRAW BENCH

C H A P T E R - 4

RESULTS AND DISCUSSION

4.1 PRELIMINARY EXPERIMENTS

After modifing the lathe as a draw bench and fixing the dynamometer rigidly on to it, sample lead rods were drawn to find out if the rods could be drawn using the set-up at different drawing speeds without necking. It was found that up to speeds of about 60 mm per minute no visible necking occurred but beyond this speed the rod could not be drawn because of instantaneous neck formation. The recorder connected to the dynamometer also indicated sufficient sensitivity in both the channels. The entire set up appeared to perform reasonably satisfactorily below drawing speeds of 60 mm per minute and this speed was therefore taken as the upper limit.

Since the speeds were to be obtained by suitable gear combinations, the following four speed steps were considered in view of availability : 16.93, 25.4, 39.69 and 50.8 mm per minute.

The test sample, having been drawn through the die, was separated into two halves and the lines inscribed on one of the interfaces (halves of the rod) were examined under a shadow-graph. The most suitable magnification for the specimen turned

out to be 10 as the entire deformation pattern could be brought into focus of the shadow graph field.

The basic requirement of Visioplasticity technique is the availability of instantaneous deformation pattern. To obtain this, a quick stop mechanism is required to 'freeze' the flow pattern inscribed on the work piece. In the present set up, this was achieved by suddenly disengaging the carriage from the lead screw which provides the motion to the carriage. The disengagement was carried out when the output on the recorder indicated a constant load, that is, when a steady state was reached. ✓

4.1 EXPERIMENTAL CONDITIONS

The experimental conditions for the present work were as under :

Work material : Lead (stress-strain curve from compression tests is shown in Fig. 3.11); Diameter : 12.5 mm.

Die : (a) Material : High carbon steel. (Manufactured from two separate pieces of high carbon steel, so that it may be separated into two pieces at the dimetral plane).

(b) Angle : Half angle 3 degrees

Cone angle 6 degrees

(c) Effective width : 12.5 mm.

Drawing speeds: 16.93, 25.4, 39.69 and 50.8 mm per minute

Drawing environment : Dry air.

4.3 EXPERIMENTAL RESULTS

The rods were drawn at four different speeds and their steady-state loads were recorded on the strip charts of the recorder. Once the steady-state was reached each drawing operation was quickly terminated to obtain instantaneous deformation pattern as depicted by the inscribed grid lines. The following results were obtained at different speeds

Drawing Speed (mm/min.)	Drawing Force (Kg.)	Separating Force (Kg.)
16.93	73.35	8.02
25.40	80.02	16.01
39.69	88.35	22.01
50.80	96.69	28.01

The variations of the drawing force and the separating force with the drawing speed are shown graphically in Fig. 4.1. It is clear that both the drawing and separating forces increase with increase in the drawing speeds. The rate of increase also appears to be constant in the range of speed considered and agrees with the published results [12] .

Fig. 4.2 shows a typical deformation pattern obtained at the drawing speed of 25.4 mm per minute. This plot was obtained directly from the lines inscribed on the work piece after it was magnified ten times on a shadow graph. As is clearly visible, the plot is 6.0 centimetre at the inlet stage and 5.4 centimetres at the outlet stage. This works out to be exactly 10 per cent reduction in radius as it should be with a die of half angle 3 degrees and 12.5 mm effective width.

4.4 ANALYTICAL RESULTS

By the use of Visioplasticity technique, the complete velocity field, the strain rate field and the stress field for rod drawing, for a drawing speed of 25.4 mm per minute are obtained and are tabulated in Table II (Page 63), Table III (Page 64) and Table IV (Page 65) respectively. The graphical representation of the drawing stress inside the deforming region is shown in Fig. 4.3.

Using the stress field thus obtained, theoretical separating force was evaluated as 15.24 Kgs. as against 16.01 Kgs. obtained experimentally.

4.5 DISCUSSION

To evaluate the strain rate field and from it the stress field inside the deforming region of the die an analytical method is developed. The details of this method are given in Appendix B. By this method, velocity field, strain rate field and stress field can be obtained with the use of a deformation pattern and an electronic calculator; without the use of an elaborate computing system. Although four different deformation patterns were obtained for four different speeds, only one was chosen for the complete analysis.

The drawing stress at various sections of the die is plotted in Fig. 4.3. For evaluation of σ_z, the load constant K in equation (A_2.7), is assumed to vary linearly along the

length of the die with zero value at the mouth and maximum at the exit. It is seen from Fig. (4.3) that the value of σ_z increases as the material advances into the die, reaching the plastic limit where the deformation takes place. The maximum deforming region is between $\frac{1}{5}^{th}$ to $\frac{2}{5}^{th}$ of the total distance between the split plane of the rod and the inner surface of the die. This agrees with common reasoning because the maximum stress would be between two interfaces where a longer time is required to reach the plastic deformation condition because of criteria like slip, interface lubrication etc.

Finally the separating force evaluated by this method is in good agreement with the separating force evaluated by the method developed.

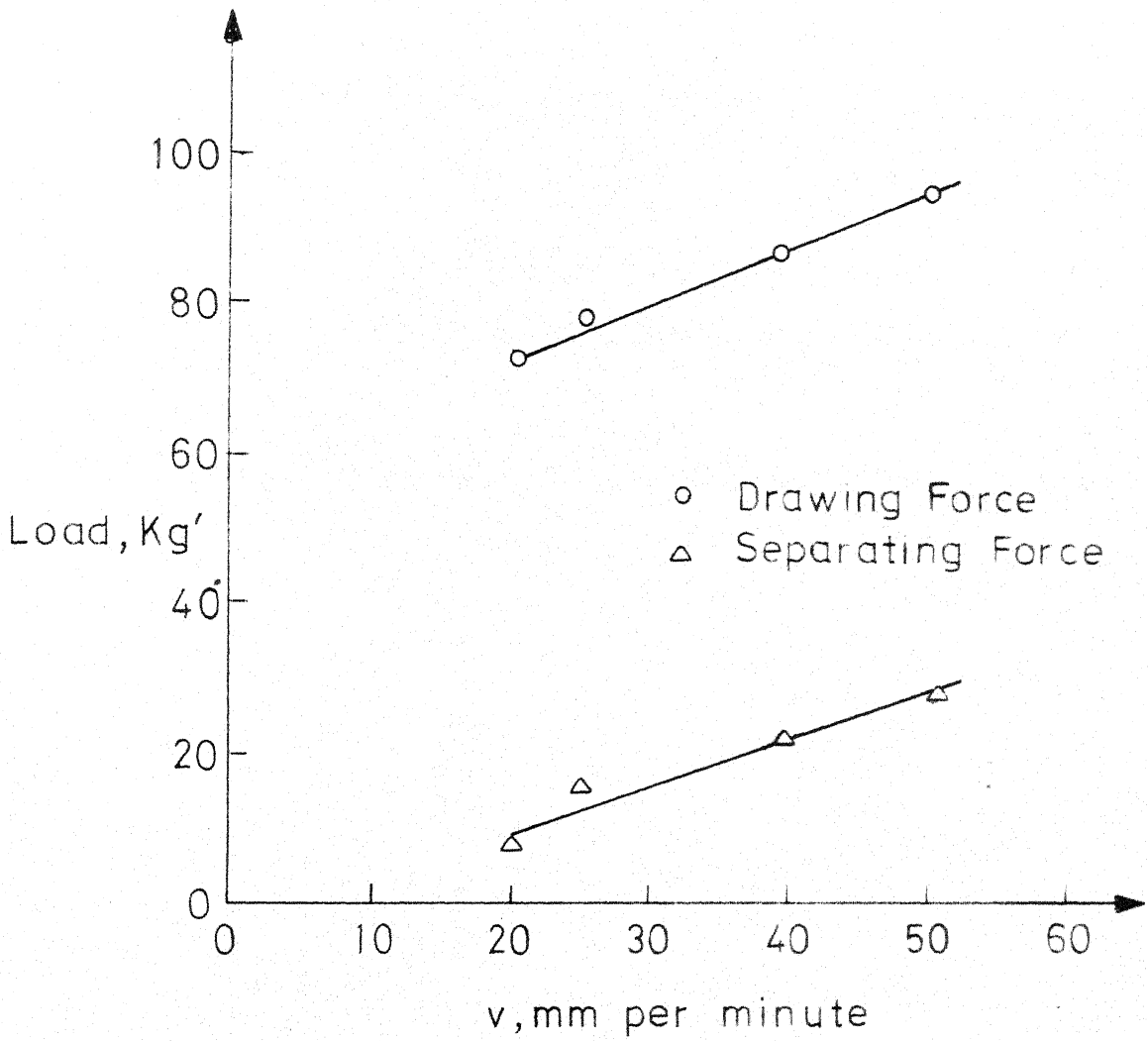

Fig. 4·1 Variation of drawing and separating forces with the variation in speed

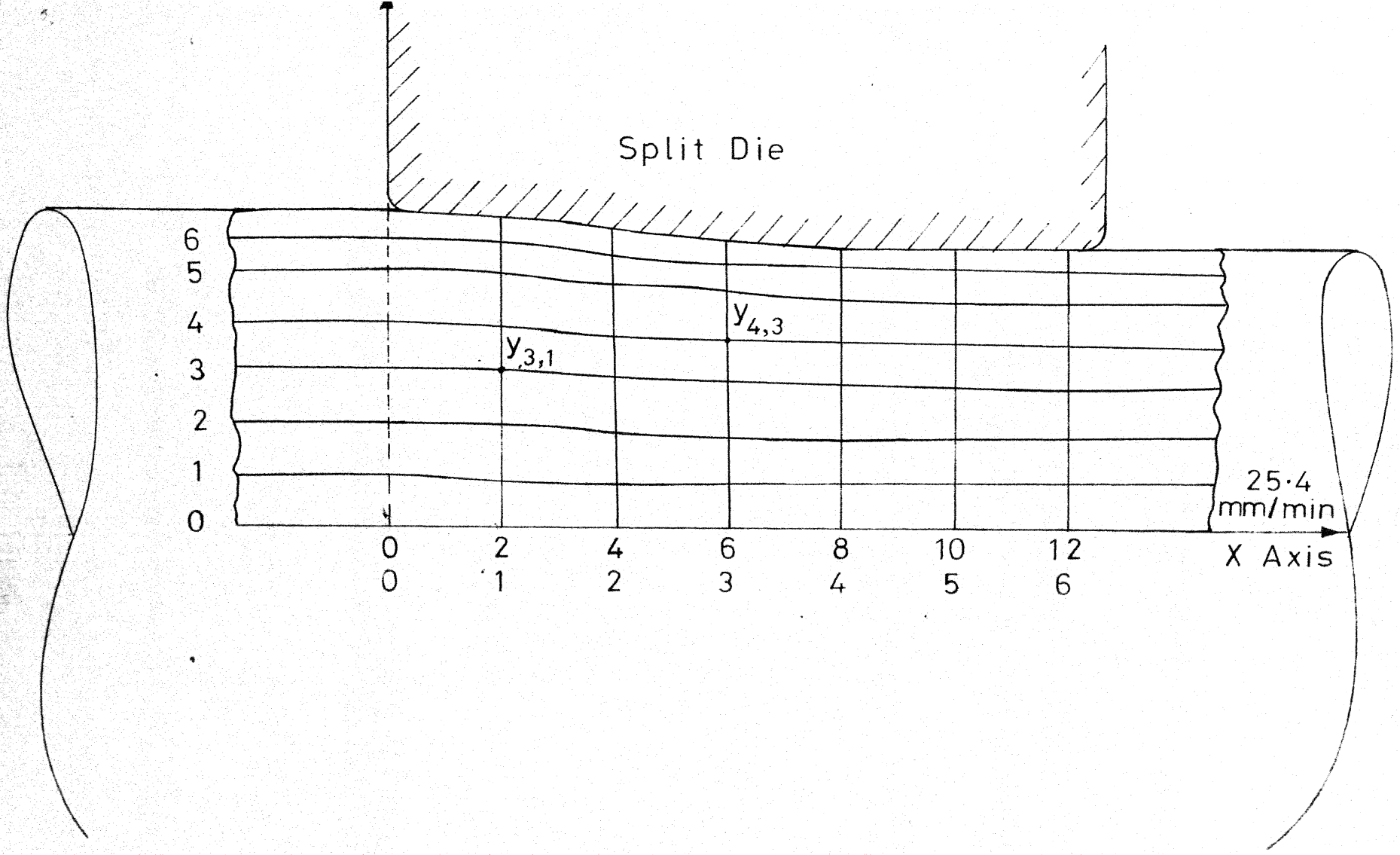

Fig.4·2 10X Deformation pattern

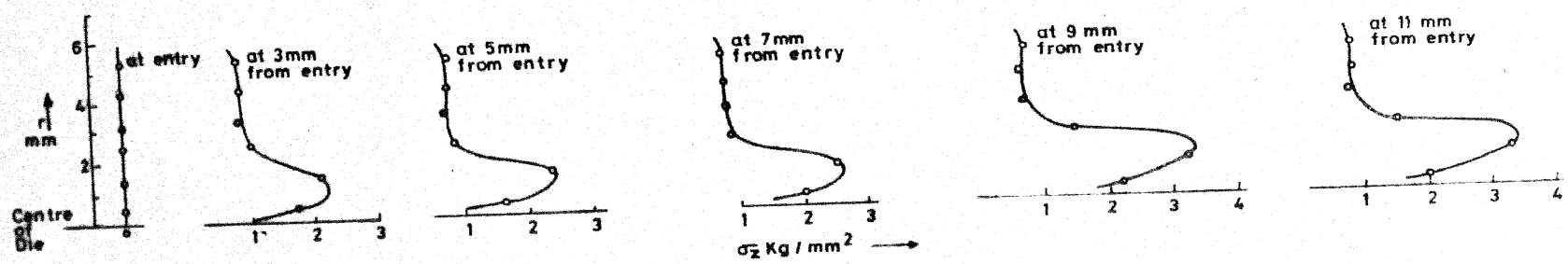

Fig.4-3 Variation of drawing stress inside the split die

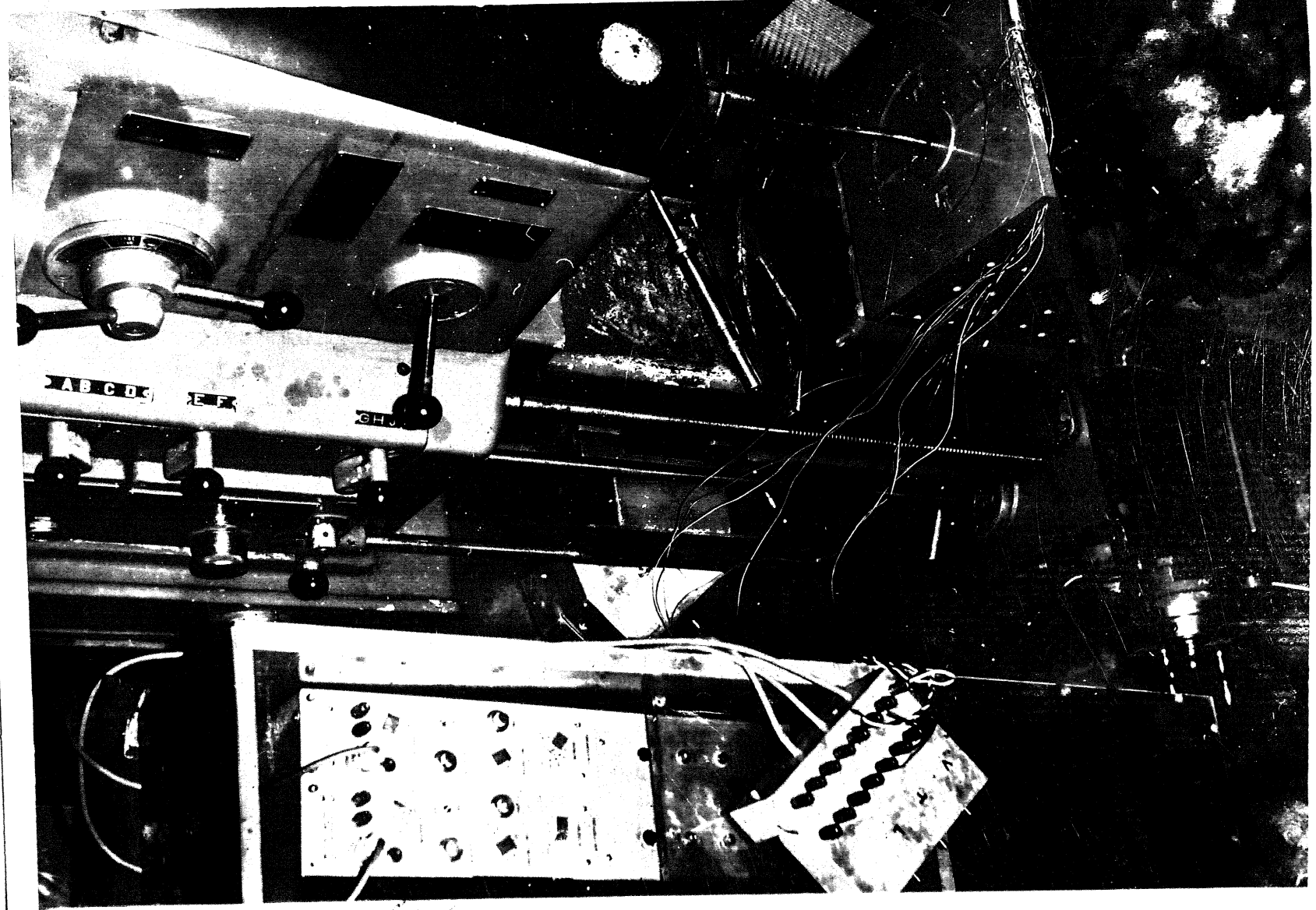

FIG. 4.4 THE EXPERIMENTAL SET UP

C H A P T E R - 5

CONCLUSIONS

A viscoplasticity technique for analysing the rod drawing process has been proposed. For this analysis the required factors are a) the steady state deformation pattern of flow lines, b) the drawing velocity and c) the flow stress. The velocity field is obtained by flow function approach which is based on the volume constancy condition. The drawing force is obtained after numerical solution of the velocity field. The forces predicted by this method agree reasonably well with the experimental values.

The disc dynamometer designed for obtaining the experimental values of drawing and separating forces has also worked satisfactorily and has such a design that it may be used for either rod drawing or wire drawing.

The technique as used is for axisymmetric drawing of isotropic materials. The analysis can, however, be modified for anisotropic materials and for cases where drawing force is nonuniform either because of draw bench design or non-homogenuity of the material being drawn. Further the analysis is limited to plastic zone only and no attempt has been made to extend the analysis in the elastic region just at the mouth of the die.

The present work can be extended to study the effects of various parameters on rod or wire drawing.

R E F E R E N C E S

1. G. Sachs, "Plasticity Problem in Metals", Trans. Faraday Soc., 24, 84 (1928).

2. P.M. Cook and J.G. Wistreich, "Measurement of die Pressure in Wire Drawing by Photo-elastic Methods", J. Appl. Phys., 3, 1 (1952).

3. E.G. Thomsen and J.T. Lapsley, "Experimental stress Determination within a Metal druing Plastic Flow", Proc. of the Soc. for Exp.Str. Ana., 11, 59 (1954).

4. A.H. Shabaik and E.G. Thomsen, "Computer Application to the Visioplasticity Method" , Trans. of Amer. Soc. Mech. Engrs., J. of Engg. for Ind., 89, 339 (1967).

5. W.B. Palmer and P.L.B. Oxley, "Mechanics of Orthogonal Machining", Proc. Inst. Mech. Engrs., 173, 623 (1959).

6. N.N. Zorev, et al., "Stresses in the Chip Formation Zone", Russ. Eng. J. 49, 81 (1969).

7. M.N. Das, R.K. Ghosh and A. Ghosh, "A new approach to the Visioplasticity Technique for solving Plastic flow Problems" , Indian J. of Tech., 9 242 (1971).

8. T.H.C. Childs, "A new visioplasticity technique and a study of Curly Chip Formation", Int. J. of Mech. Sci., 13, 373 (1971).

9. W. Des Santos and A.J. Organ, "Deformation of the Ductile Fracture Processes examined by the Visioplasticity method", Int. J. of Mach. Tool Design and Research, 13 217 (1973).

10. K. Okushima and K. Hitomi, "A design of a three component Tool Dynamometer" Memoirs of the Faculty of Engineering, Kyoto Univ., 23, 321, (1961).

11. G.L. Baraya, "Mechanical and Photographic Processes for Producing a Grid of Lines", Int. J. of Mech. Sci., 5, 365 (1963).

12. C.T. Yang, "On the Mechanics of Wire Drawing", Trans. ASME, Series B, J. Eng. Ind., 83 523 (1961).

A P P E N D I X - A

A Hindustan centre Lathe LB 17 (manufactured by Hindustan Machine Tools Ltd., Bangalore 31), was modified to work as a draw bench. It had the following specifications.

Height of centre	170 mm
Type of bed	Straight bed
Centre distance	1,000 mm.
Swing over bed	350 mm.
Swing over cross slide	170 mm.
Bed width over top surface	312 mm
Spindle bore	42 mm
Tapre in bore	Metric 50
Reducing gear	1:4 and 1:14
Standard range	45-2000 rpm(10 HP/3000 rpm moto)
Slow range	23-1000 rpm(7 HP/1500 rpm motor)
Tail stock sleeve dia	70 mm
Tail stock taper in bore	Morse taper no. 4
Lead screw pitch	6 mm (4 TPI).

APPENDIX - B

To obtain a velocity field, and then the stresses at various sections of the conical die, a numerical method was developed. This method does not require the use of an elebrate computing system and can evaluate stresses in the deforming region with the help of an electronic calculator.

The grid lines in the deformed region are magnified ten times and traced on a graph paper. This fixes the coordinates of all the points of various lines with respect to the central line (x-axis). The y axis is choosen parallel to the entry face of the die. For fixed values of x(0,2,4,6 etc. mm) values of the y cordinates for the specific lines are read off. This gives the position of the lines in tabular form (Table I).

The drawing speed of the rod is a known parameter. Using volume constancy this velocity is transferred to the entry side. The entire mass of the rod is divided into tubes encampassed by the lines drawn on the specimen. Volume of each of these tubular sections V_i at various values of x is calculated, using the formula

$$V_i = \pi(y^2_{i+1,j} - y^2_{i,j}) \times \text{segment length} \qquad (A_2.1)$$

$i = 0$ to 6 (or number of lines)

$j = 0$ to 6 (or number of segments)

Refer Fig. 4.2.

Using volume constancy, velocity in a particular section can be evaluated. Since the inclination of the mid point line of a particular section is directly measured, the horizontal and vertical velocities at each section can be evaluated. That is, if velocity at a previous section is known the velocity to the immediately next section is given by the formula

$$V = V_o\left(\frac{y^2_{i+1,j} - y^2_{i,j}}{y^2_{i+1,j+1} - y^2_{i,j+1}}\right) \cos\theta \qquad (A_2.2)$$

V = new velocity, θ = angle of inclination

V_o = velocity in the previous section

i, j as in eq. $A_2.1$

This directly gives the velocity distribution field inside the die. A typical velocity distribution for drawing velocity of 25.4 mm per minute is shown in Table II.

Evaluation of velocity field by this method is unlike the conventional method as the complete velocity field is determined from one single steady state deformation pattern. The main assumption in this method is that the increment of velocity in each interval is linear, but the average velocity in each interval is kept the same. The same velocity cannot differ much from actual velocity, as the errors are always of compensating type [7].

Having obtained the velocity field, the strain rate field inside the split die is obtained numerically. Analysis of

T A B L E - I

Tabular representation of the deformed grid lines

	x_0 0	x_1 2	x_2 4	x_3 6	x_4 8	x_5 10	x_6 12
y_0	0	0	0	0	0	0	0
y_1	1.0	0.90	0.83	0.8	0.80	0.80	0.80
y_2	2.0	1.9	1.85	1.8	1.72	1.70	1.70
y_3	3.1	3.0	2.9	2.8	2.7	2.68	2.68
y_4	4.0	3.85	3.7	3.6	3.5	3.45	3.45
y_5	5.0	4.85	4.68	4.5	4.4	4.3	4.3
y_6	6.0	5.8	5.6	5.5	5.45	5.4	5.4

T A B L E - II

Tabular representation of velocity field

x	0-0	0-2	2-4	4-6	6-8	8-10	10-12
V	18.96	23.42	27.54	29.63	29.63	29.63	29.63
u	18.96	23.41	27.53	29.63	29.63	29.63	29.63
v	0	-0.59	-0.48	0	0	0	0
$(-\theta^{o})$	0	1.432	1.003	0.430	0	0	0
V	18.96	20.31	20.73	21.74	24.35	25.08	25.08
u	18.96	20.29	20.70	21.74	24.35	25.08	25.08
v	0	-1.01	-1.24	-0.43	-0.12	0	0
$(-\theta^{o})$	0	2.862	3.434	1.146	1.146	0.287	0
V	18.96	19.47	21.31	23.02	24.4	24.62	24.62
u	18.96	19.72	21.30	23.00	24.38	24.62	24.62
v	0	-0.99	-0.80	-0.86	-1.10	-0.25	0
$(-\theta^{o})$	0	2.862	2.148	2.148	2.577	0.573	0
V	18.96	20.90	22.98	23.66	24.37	25.57	25.56
u	18.96	20.50	22.94	23.63	24.34	25.56	25.50
v	0	-1.30	-1.43	-1.18	-1.22	-0.45	0
$(-\theta^{o})$	0	3.577	3.577	2.862	2.862	1.002	0
V	18.96	19.58	20.79	23.45	24.12	26.04	26.04
u	18.96	19.53	20.70	23.39	24.09	26.02	26.04
v	0	-1.46	-1.66	-1.64	-1.20	-0.98	0
$(-\theta^{o})$	0	4.289	4.574	4.004	2.862	2.148	0
V	18.96	20.75	22.22	21.06	20.33	19.71	19.71
u	18.96	20.67	22.12	21.01	20.32	19.69	19.69
v	0	-1.81	-2.05	-1.47	-0.76	-0.74	0
$(-\theta^{o})$	0	5.006	5.285	4.004	2.148	2.148	0

All the velocities are in mm per minute.
All the angles are in degrees.

T A B L E - III

Tabular representation of strain distribution inside the split die

x	0-2	2-4	4-6	6-8	8-10	10-12
y	1.0	0.9	0.83	0.8	0.8	0.8
$\dot{\epsilon}_z$	1.06	1.06	1.06	1.06	0.0	0.0
$\dot{\epsilon}_r$	0.0	-0.23	-0.29	-0.35	-0.22	-0.21
$\dot{\gamma}_{zr}$	0.0	-0.42	-0.77	-1.16	-1.46	-1.50
y	2.0	1.9	1.85	1.80	1.72	1.70
$\dot{\epsilon}_z$	0.63	0.63	0.63	0.63	0.63	0.63
$\dot{\epsilon}_r$	0.0	-0.23	-0.29	-0.35	-0.22	-0.21
$\dot{\gamma}_{zr}$	0.0	-0.40	-0.75	-1.14	-1.44	-1.50
y	3.1	3.0	2.9	2.8	2.7	2.68
$\dot{\epsilon}_z$	0.63	0.63	0.63	0.63	0.63	0.63
$\dot{\epsilon}_r$	0.0	-0.23	-0.29	-0.35	-0.22	-0.21
$\dot{\gamma}_{zr}$	0.0	-0.47	-0.82	-1.21	-1.51	-1.50
y	4.0	3.85	3.7	3.6	3.5	3.45
$\dot{\epsilon}_z$	0.63	0.63	0.63	0.63	0.63	0.63
$\dot{\epsilon}_r$	0.0	-0.23	-0.29	-0.35	-0.22	-0.21
$\dot{\gamma}_{zr}$	0.0	-0.48	-0.83	-1.22	-1.52	-1.50
y	5.0	4.85	4.68	4.5	4.44	4.3
$\dot{\epsilon}_z$	0.74	0.74	0.74	0.74	0.74	0.74
$\dot{\epsilon}_r$	0.0	-0.23	-0.29	-0.35	-0.22	-0.21
$\dot{\gamma}_{zr}$	0.0	-0.51	-0.86	-1.25	-1.55	-1.50
y	6.0	5.8	5.6	5.5	5.45	5.4
$\dot{\epsilon}_z$	0.68	0.68	0.68	0.68	0.68	0.68
$\dot{\epsilon}_r$	0.0	-0.23	-0.29	-0.35	-0.22	-0.21
$\dot{\gamma}_{zr}$	0.0	-0.6	-0.95	-1.34	-1.64	-1.50

T A B L E - IV

Tabular representation of stress distribution inside the split die

x	0	3	5	7	9	11
r	0.5	0.45	0.42	0.40	0.40	0.40
σ_z	0.0	1.70	1.87	2.03	2.21	2.00
σ_r	0.0	-2.07	-1.93	-1.67	1.38	1.23
r	1.5	1.40	1.34	1.30	1.26	1.25
σ_z	0.0	2.08	2.36	2.51	3.25	3.30
σ_r	0.0	-2.12	-1.61	-1.09	0.55	0.70
r	2.55	2.45	2.38	2.3	2.21	2.19
σ_z	0.0	0.98	0.82	0.76	1.47	1.53
σ_r	0.0	-3.19	-3.05	-2.71	-1.16	-1.07
r	3.55	3.43	3.3	3.2	3.10	3.07
σ_z	0.0	0.80	0.71	0.72	0.58	0.66
σ_r	0.0	-3.3	-3.16	-2.71	-2.02	-1.94
r	4.5	4.35	4.19	4.05	3.95	3.88
σ_z	0.0	0.84	0.77	0.80	0.63	0.74
σ_r	0.0	-3.16	-3.03	-2.73	-2.10	-2.03
r	5.5	5.33	5.14	5.00	4.93	4.85
σ_z	0.0	0.83	0.8	0.8	0.7	0.75
σ_r	0.0	-1.87	-1.37	-1.0	-0.43	-0.5

All the stress are in Kg. per square mm. x and r are coordinate of intersection of mid-point lines of grid lines and vertical lines drawn at equal spacings along the x-axis (z-axis).